DEPARTMENT OF ASTRO-GEOPHYSICS

UNIVERSITY OF COLORADO, BOULDER, COLORADO 80309

SOLAR RADIO EMISSION

Martin V. Goldman* and Dean F. Smith**

Draft of review paper for the
National Academy of Sciences
Space Science Board's Study on
The Physics of the Sun

CU #1042

Department of Astro-geophysics
University of Colorado
Boulder, CO 80309

May 1981

*Author of Sections 2.1 and 3

**Author of Sections 2.2-5, 4 and 5

1. INTRODUCTION

The subject of solar radio emission is quite broad and has been reviewed repeatedly in articles and books, (Wild, Smerd, and Weiss, 1963; Kundu, 1965; Zheleznyakov, 1970; Wild and Smerd, 1972; Rosenberg, 1976; Smerd, 1976; Melrose, 1980a). In addition recent conference proceedings include issue 9 of Radiophys. Quantum Electron. 20 (1977) and Radio Physics of the Sun (Dordrecht, Reidel, 1980). Whole books exist on specialized topics. We shall refer to them as necessary.

Because of this wealth of material, no attempt will be made in this review at completeness, either as concerns subject matter or references. Rather, we have selected a number of topics which are present active areas of both observational and theoretical research. New observational and theoretical material is forcing the re-examination of present ideas and in many cases the development of new theories. This sensitive interplay between observations and theory is vital to the further development of the field. We have chosen some of the topics where rapid progress is being made in our physical understanding of the phenomenon or could be made in the near future.

We begin with a brief review of the range of phenomena in the field as shown schematically in Figure 1.1. This is a dynamic spectrum or frequency versus time plot. Assuming that

the frequency is related to the electron plasma frequency $\omega_p = (4\pi ne^2/m)^{1/2}$, where n is the electron density, the dynamic spectrum can also be converted into a height versus time plot as shown on the right hand side of Figure 1.1. This is the reason that decreasing frequency is plotted on the left. Active regions on the sun continuously produce type I noise storms in the range 40-400 MHz and low-frequency type III bursts as shown on the left of Figure 1.1. Superimposed on the continuum of the type I noise storms are brighter type I bursts [see, e.g., Fig. 5 of Smerd (1976)] which are narrow in bandwidth as indicated by the dashed lines in the center of Figure 1.1 which would have been better labeled "I storm bursts." When a large flare occurs, a continuum microwave burst is produced at the flashphase (the phase in which most emissions increase most rapidly), which may be followed by a microwave type IV burst which lasts 30 min to 1 hour. A flare associated type III burst is also produced at the flashphase which usually extends to higher frequencies than low-frequency type III storm bursts and is more intense at meter wavelengths. It may have a continuum attached to it which is not shown and called a type V burst. Type III bursts are also known as fast-drift bursts because of the rapid rate at which the bursts drift from high to low frequencies. The type II burst also starts at the flashphase and is split into two bands as are a few high frequency type III bursts; the lower

frequency one is called the fundamental because of radiation near ω_p and the upper frequency one is called the second harmonic because of radiation near $2\omega_p$. Type II bursts have a slow drift rate.

Several minutes after the flashphase, a metric type IVm burst which is a continuum burst may develop. It can be connected to the microwave type IV burst by a decimeter type IVdm burst which is a combination of continuum with fine structure. These continuum bursts are all stationary, but when viewed with a radio interferometer or heliograph, a separate continuum source, the moving type IV burst may break off from the stationary type IVm and move out into the corona with a drift rate somewhat slower than for a type II burst. After this, a type I noise storm may continue for hours or days and have low-frequency type III bursts associated with it. More complete accounts of the observations of microwave, type I, type II, type III and moving type IV bursts are given in Section 2.

We now consider the physical mechanisms which give rise to these bursts. The reader is referred to Wild et al. (1963) and Smerd (1976) for arguments for these choices. Microwave bursts are caused by ≈100 keV electrons trapped in a magnetic arch and will be treated along with other bursts caused by trapped electrons in Section 5. Type III bursts are caused by dilute streams of mildly relativistic electrons (≈10-100 keV).

As such they have one of the least perturbing sources of the corona and thus represent one of the simplest phenomena. For this reason, the physics of type III bursts will be considered first in Section 3. Type II bursts are caused by collisionless shock waves which are a more perturbative phenomenon since the density increases behind the shock. A similar region of density enhancement is a current sheet between two oppositely directed magnetic fields. The physics of type II bursts and their related shocks is considered in Section 4. Some type I bursts may be associated with current sheets. Alternately type I bursts may be caused by electrons trapped in a magnetic arch or loop which is a region of higher density than the normal corona. Occasionally, part of this loop is blown off by reconnection processes and we see a white-light coronal transient. This is the most perturbing type of source and is often associated with a moving type IV burst. Sometimes these bursts appear to come from their own self-contained plasmoid which is a trap for the emitting electrons. The physics of both stationary and moving traps and the associated microwave, type I and moving type IV bursts are considered in Section 5.

In Section 6 we consider the status of the field of solar radio emission, where it is going and what will be needed to insure its future health. We have not considered how the radiating electrons are accelerated since this is covered in a separate review in this volume.

2. OBSERVATIONAL RESULTS

2.1. Type III Bursts

2.1.1. Ground-based observations (above ∿8 MHz)

The discussion of type III radio bursts (Wild, 1950a,b; Wild and McCready, 1950) was enabled by the dynamic radio-spectrograph (Sheridan, 1967; Dulk and Suzuki, 1980), which records contours of equal flux (intensity per frequency-interval) on a frequency-time plot. The drift rate, defined as the time rate of change of frequency, f, is given roughly by $f^{1.85}/(100\ \text{sec})$, for type III bursts, with f in MHz. This formula holds from 10^3 MHz, all the way down to 0.1 MHz (Alvarez and Haddock, 1973), corresponding to electron streams with velocity between 0.2c and 0.6c. The lifetime of a time profile at f ≈ 80 MHz is 3-5 s. A typical time profile is characterized by a rapid rise, and a slower, approximately exponential decay of form $\exp(-10^{-8} f\ t)$ (Wild, 1950a). Recent measurements yield flux densities of the order of a few times 10^{-19} W m^{-2} Hz (Dulk and Suzuki, 1980). For a fully-resolved source (Melrose, 1980), this corresponds to average brightness temperatures of 10^{10} °K at 80 MHz and 3×10^{10} °K at 43 MHz (Dulk and Suzuki, 1980).

Bursts commonly occur in groups of ten or more, with a separation of seconds (Wild et al., 1963; McLean, 1971). This is probably a manifestation of an interrupted stream of

electrons in the lower corona. It seems quite certain (Smerd, 1976) that fundamental-harmonic pairs can be distinguished from groups of bursts. In Figure 2.1 we see a number of such pairs, recorded in 1954. The existence of the harmonic lends strong support to the early hypothesis that resonant electron plasma (Langmuir) waves are involved in type III emissions. At first, such pairs were only found in about 10% of bursts (Wild et al., 1954), but recent measurements show that they may comprise a significant fraction of type III bursts in the frequency range from 30-210 MHz (Dulk and Suzuki, 1980). The fundamental usually begins below 100 MHz, while the harmonic component can begin from a frequency as large as 500 MHz (Dulk and Suzuki, 1980). The wide frequency bandwidth at any given time is due to the wide range of plasma frequencies encountered by the electron stream at that instant, and the relatively slow decay times of frequencies excited earlier. The frequency ratio between the two bands generally is of the order of 1.85, and never exceeds 2. This has been attributed to a "chopping-off" of the lowest frequencies, f, of the fundamental band, due to reflection by small density irregularities, whose plasma frequency, f_p, rises above f (Roberts, 1959; Riddle, 1972, 1974; Stewart, 1974).

In Figures 2.1(d) and 2.1(e), the drift to lower frequencies slows to a halt. In other cases (not shown), the drift can reverse towards higher frequencies after stopping.

Due to the appearance of such bursts on spectrograms in which time is on the horizontal axis, and the frequency is plotted vertically, they are called J and U bursts (Stewart, 1975). A likely explanation for such bursts is that they are generated by electron streams which follow closed magnetic field lines, and sample higher densities first, then lower densities higher in the corona, and finally higher densities lower in the corona. Such events have even been seen from satellites, at frequencies as low as 800 kHz, corresponding to closed magnetic loops of size 35 $R_\odot$ (Fainberg and Stone, 1974).

For normal type III bursts associated with streams which travel along open field lines, the drift to lower frequencies continues indefinitely, due to the stream front encountering progressively lower densities as it travels along an open magnetic field line.

In order to determine whether the emission corresponds to a local plasma frequency or twice the local plasma frequency it is necessary to identify the true source height in the corona and to associate the correct electron plasma density with that height. This has proven to be a difficult and elusive task both at high (>10 MHz) and at low (10 MHz > f > 10 kHz) frequencies.

At 43, 80 and 160 MHz the radioheliograph (Wild, 1967; Sheridan et al., 1973) may be used to record the apparent position, shape and polarization of type III bursts. In

Figure 2.2, we see the apparent source regions for a fundamental-harmonic pair in a type III burst at the limb, for these three frequencies. It is reassuring that the lower frequencies appear to emanate from higher altitudes, but the apparent heights probably do not coincide with true source heights, due to refraction and scattering effects in the propagation of the emission. Refraction shifts the apparent fundamental position outwards, and the harmonic inwards (McLean, 1971; Riddle, 1972). A simple correction for this effect (Stewart, 1976) still yields coronal electron densities which need to be an order of magnitude larger than quiet sun values at solar minimum (Saito, 1970), in order for the plasma frequencies of the true source heights to correctly correspond to the observed frequency for fundamental emissions and to one-half the observed frequency for harmonic emissions. To some extent, the radio bursts are likely to be generated in dense coronal structures such as loops and streamers. A ducting mechanism, proposed by Duncan (1979), helps to bring observed frequency-height correlations more into line with the quiet sun density profile, but enhanced streamer densities are probably still necessary.

It is fairly certain that the apparent source sizes are larger than the true source sizes. The discrepancy is probably due in part to scattering of the emission from small scale density irregularities (Riddle, 1972) but this cannot be the

whole story. A close examination of Figure 2.2 reveals a number of surprises. First the apparent source size rapidly increases as the frequency decreases (see also Dulk and Suzuki, 1980). Second, at a given frequency (say 80 MHz) the apparent height and size of the fundamental source (dashed medium line) is nearly identical to the apparent height of the harmonic source (solid medium line) which arrives later (Smerd et al., 1962; Bougeret et al., 1970; McLean, 1971). Third, at a given time, the source of the fundamental (at say 80 MHz) is observed at a greater apparent height than the source of the harmonic (at 160 MHz), even though the two frequencies should be emitted from the same volume of space. All of these features are explained by Duncan's (1979) mechanism of radio-wave ducting by radially-elongated density inhomogeneities, together with the assumption of extremely divergent open magnetic field lines (Dulk, Melrose and Suzuki, 1979). This latter assumption also fits in nicely with satellite observations of sources of low frequency emission near the Earth, in which a source size of 1 AU is observed (Fainberg and Stone, 1971).

The radioheliograph and spectropolarimeter (Suzuki, 1974) have provided valuable information concerning the polarization of type III bursts in the range from 24 to 220 MHz. At the fundamental, the average degree of circular polarization is 35% (Dulk and Suzuki, 1980; Suzuki and Sheridan. 1977), although, at lower frequencies, almost

complete polarization has occasionally been observed (Hanasz, et al., 1980). The sense of polarization is consistent with emission in the o-mode of magneto-ionic theory (Melrose, 1980a). At the second harmonic, the average degree of polarization is 11%, and the sense is the same; however, if the second harmonic lasts longer than one minute, then the sense of polarization reverses, possibly due to emission in the x-mode (Dulk, 1980b). For any given harmonic-fundamental pair, the degree of polarization is always greater for the fundamental. Another important fact is that, on the average, the degree of circular polarization decreases for all bursts from center to limb (Dulk, et al., 1979; Dulk and Suzuki, 1980).

A small percentage of type III bursts are followed by continuum radiation, known as type V emission. The type V emission has some of the character of the type III. It is thought to be second harmonic plasma emission from an abnormally slowly propagating or widely dispersed beam (Melrose, 1974), since it exhibits such a slow drift. Its most unusual characteristic is that it has the opposite polarization (but the same degree) as the second harmonic in type III bursts (Dulk et al., 1980b).

2.1.2. Spacecraft observations (below 1 MHz)

The study of general properties of bursts below about 5 to 10 MHz usually is not possible from earth-based radio

receivers, due to the maximum electron density in the ionospheric F-layer, which causes total reflection away from the Earth. Since about 1964, but especially in the last decade, important satellite measurements have been made at a variety of radial distances from the sun, between 0.3 AU (Helios 1 and 2) to 1.2 AU and beyond (Voyager 1 and 2).

In order to observe the solar radio emissions, the spacecraft would be equipped typically with a dipole antenna (of length 30-120 meters) and multichannel spectrum analyzer which together comprise a satellite radio spectrograph. In Figure 2.3, we see the characteristic drift from high to low frequencies, here laid out as a sequence of time-profiles. Each is again characterized by a rapid rise and a slower, approximately exponential decay. At the lower frequencies the burst extends over minutes or hours, instead of the seconds associated with ground-based observations. This data comes from an in-depth study and summary of early earth-orbiting satellite results by Fainberg and Stone (1974). The observation made by Wild that the decay in time of any frequency component is exponential over many decades holds true for the low frequency bursts as well, and his decay formula need only be slightly modified to cover the frequency range from 2.8 MHz down to 67 kHz. Evans et al. (1973) find an approximate decay as exp $-(0.5 \times 10^{-8} f^{1.09} t)$. Attempts to explain the decay in terms of collisional damping (free-free

absorption) of the emission by a thermal background plasma do not seem to give the correct temperature near 1 AU (Evans et al., 1973; Haddock and Graedel, 1970; Fainberg and Stone, 1974). The excitation time, t_e, from burst onset to maximum can be fitted (Evans et al., 1973) by $t_e = 4 \times 10^8/f^{1.08}$, with f in hertz.

Due to antenna rotation on a spin-stabilized spacecraft, the received radiation shows a definite modulation pattern (Figure 2.3). Hence, one can determine the direction of arrival of a given frequency component of a burst, in the plane defined by the rotating dipole. This is known as the spin modulation technique, and it can be used to help determine the source location of the low-frequency bursts (Slysh, 1967; Fainberg and Stone, 1974).

There are a number of problems involved in locating the source for each frequency, associating a local density and plasma frequency with that location, and deciding whether the corresponding emission is fundamental or second harmonic. However, if these determinations can be made, one can, in principle, construct the dynamical trajectory of the exciting electron stream. The stream is guided by open solar magnetic field lines, so the trajectory of sources for a sequence of decreasing frequencies can be expected to follow the Archimedes spiral (Parker, 1958) of the field line. Fainberg et al. (1972, 1974) constructed source trajectories for a number of

type III bursts. Spin modulation gave the direction of arrival projected onto the ecliptic plane. This defined for each frequency a line of possible source locations in the ecliptic plane, emanating from the spacecraft. The location of the source on that line was determined by a model for the average emission frequency as a function of radial distance from the sun:

$$f_{obs} = 66.8\ R^{-1.315} \qquad (2.1.1)$$

where f is in megahertz and R is distance to the sun in solar radii, $R_\odot$. The resulting source trajectory closely matched the expected Archimedean spiral form of the magnetic field in the solar wind. Using a very crude model for the electron density profile as a function of radius, they were able to show that the associated profile of plasma frequencies was only slightly lower than the profile of half-frequencies determined from the observed frequency profile. From this they concluded that the observed burst was second harmonic emission from about 400 kHz down to 30 kHz. This, together with other evidence based on type II bursts and also on the absence of spin modulation at twice the local plasma frequency at the site of the IMP-6 satellite led them to the conclusion that most type III bursts below 1 MHz are second harmonic.

It is important to note that, in many thousands of observed low-frequency type III bursts, they found no cases in which both fundamental and harmonic components were observed.

Haddock and Alvarez (1973) interpreted most complex type III events observed on OGO-5 as making a transition from predominantly fundamental to predominantly harmonic, below about 1 MHz. They identified the emission as fundamental or second harmonic by the time delay in its arrival. Using the same analysis for type III bursts observed from the IMP-6 satellite, Alvarez et al. (1974) found the transition from fundamental to harmonic occurred at 230 kHz. Recently, Kellogg (1980), using similar ideas, found the transition as low as 50 kHz in one burst observed from the solar orbiting Helios 2 spacecraft.

Gurnett et al. (1978) eliminated some of the uncertainties in the above analyses, by using the solar orbiting Helios 1 and 2, together with the IMP-8 and Hawkeye 1 satellites to measure the source locations and (a few days later) the in-situ densities and plasma frequencies along the source trajectory. This enabled a comparison to be made between the measured plasma frequencies and the observed emission frequencies. It appeared that the burst was second harmonic, rather than fundamental, at the measured frequencies, thus supporting the conclusions of Fainberg et al. (1974).

The peak intensity of a given low frequency component of a burst can be quite high. Evans et al. (1971) found the brightness temperatures for the 1 MHz component of one type III burst was in excess of 10^{15}K (fluxes in excess of 2×10^{-15} W

m^{-2} Hz). However, Melrose (1980) quotes a typical brightness temperature of 10^{11}K for the 50 kHz (harmonic) component at 1 AU. In Figure 2.3, the peak intensity is largest at 185 kHz, corresponding to about 50 $R_\odot$.

A more important intensity measure is the volume emissivity, J, which is the power emitted per unit volume per unit solid angle: $J \equiv (\Delta P/\Delta V \Delta\Omega)$ W m^{-3} sr. Recently Tokar and Gurnett (Gurnett et al., 1980) compiled the volume emissivity at a number of frequencies in each of 36 low-frequency type III events observed by IMP-8 and ISEE-1 satellites. By using Equation (2.1.1), they associated a heliocentric radial distance with each emissivity. The result is shown in Figure 2.4. Variations in emissivity of over five orders of magnitude are evident at some radii, but the best power law fit is $J = J_0 R^{-6.0}$, where $J_0 = 1.5 \times 10^{-24}$ W m^{-3} sr.

2.1.3. Langmuir waves and electron streams

A fundamental question concerning the origin of type III bursts is how well they correlate with the electron streams and Langmuir waves which are supposed to produce the observed emissions. Spacecraft measurements over the past decade have verified the existence of both the electron stream and Langmuir waves.

It has been established fairly definitely that stream electrons (presumably from solar flares or other activity) are

primarily responsible for the type III radio emission (Lin, 1970, 1974; Alvarez et al., 1972; Frank and Gurnett, 1972; Lin et al., 1973; Gurnett and Frank, 1975; Lin et al., 1981). The streams have the proper speed to account for the observed drifts of the type III bursts (0.2c to 0.6c). Typical beam to background density ratios are 10^{-7}, or, at most, 10^{-6}, at energies around $\sim$25 keV.

An interesting correlation between radio flux and the flux of electrons with energies in excess of 18 keV has been demonstrated by Fitzenreiter et al. (1976) and is illustrated in Figure 2.5. They examined a number of type III events at 1 AU from the IMP-6 spacecraft at frequencies believed to be local (because of the absence of spin modulation). The onset of >18 keV electrons coincided with the onset of local emission. (Lower energy electrons arrived after the emission had peaked.) As both the flux of radio emission F_R, and the flux of high energy electrons, F_E, increased in turn, a sequence of values of F_R were plotted against F_E. Two kinds of power laws, $F_R \propto (F_E)^{\alpha}$, were found. At flux values less than 50 per cm^2-s-sr, $\alpha = 1$, whereas for flux values greater than 50 per cm^2-s-sr, $\alpha = 2.4$. In Figures 2.5(h) and 2.5(i), the transition is visible. They argue that the existence of two distinct regimes of radio emission implies a fundamental change in the emission mechanism of type III bursts when the electron flux reaches a critical level.

Very recently, more detailed studies of the electron streams were presented, based on data collected from the ISEE-3 spacecraft, 259R_e upstream from the Earth (Lin et al., 1981). In Figure 2.6(b) we see the spin-averaged electron fluxes in different energy intervals, as a function of time. In Figure 2.6(a), the measured electron field strengths are plotted simultaneously, in various wide-band frequency channels. The time profiles at 100 kHz and 56.2 kHz are interpreted as harmonic emission, and the 56.2 kHz component is identified as local because of the absence of spin modulation. (It is at roughly twice the local plasma frequency.) Two temporally consecutive bursts are evident, but only the second is of concern here. Its onset coincides with the arrival only of the electrons with energy above 200 keV, at a very low flux level. Lower energy electrons arrive progressively later due to velocity dispersion in the stream. The electric field profiles in the 31.1 and 17.8 kHz channels in Figure 2.6(a) are interpreted as electron plasma (Langmuir) waves. At energies of 20 keV and above, the pitch-angle distribution (not shown) is flat-topped and sharp-sided, whereas it is more beamlike below 10 keV.

By assuming the electron distribution function is symmetric about the magnetic field, Lin et al. (1981) were able, for the first time, to plot the electron distribution function for parallel velocities, V (integrated over all $V_\perp$).

The resulting one-dimensional distribution function is shown in Figure 2.7 in a sequence of (displaced) plots over five minute intervals. More detailed analysis shows the distribution function first develops a tiny, short-lived positive slope, $f' > 0$, at 1953 UT. This rises by two orders of magnitude around 2000 UT, and remains positive until about 2045 UT. The region of $f' > 0$ begins at $V = 1.3 \times 10^{10}$ cm s^{-1}, and moves down to $V = 3 \times 10^{9}$ cm s^{-1}, with a typical range of $\Delta V = 0.3$ V. There are several important conclusions which can be drawn from Figure 2.7. First, there is a surprising fact to note about the ambient background electron distribution [black dots in Figure 2.7(a)]. An enhanced tail of nonthermal electrons is observed at all times. This tail may be fitted approximately with an exponential distribution, having an effective temperature of around 10 keV. Second, the authors note that the onset times of large positive slopes, f', correspond very well with the onset times of Langmuir waves at 2000 UT [see Figure 2.6(a)]. This establishes for the first time the theoretically expected causal relation between the $\lesssim$25 keV part of the electron stream and (Cerenkov-emitted) unstable Langmuir waves.

However, the Langmuir waves, and the $\lesssim$25 keV electrons which produce them, are both observed about 20 minutes after the onset of the local harmonic emission, so their theoretically expected causative role in the second harmonic

emission (Section 3) would seem to be ruled out! The delay in the appearance of Langmuir waves until the harmonic emission is well underway is not unique to this event, or to observations at 1 AU. It seems to be a pervasive feature of all measurements which detect both the local second harmonic emission and the local plasma waves, including those observed in-situ near 0.5 AU (Gurnett and Anderson, 1977; Gurnett et al., 1978b).

This raises a serious theoretical challenge. The most upsetting explanation would be that Langmuir waves do not play a role in harmonic emission, although a viable alternate mechanism is unknown. Another explanation would be that the emission interpreted as local second harmonic is really fundamental, coming from much closer to the sun, but scattered significantly from density inhomogeneities to account for the observed absence of spin modulation. However, this seems contrary to most (but not all) of the observational evidence we have reviewed earlier in this section. It appears that the only other possibility is that the spacecraft somehow consistently misses the early Langmuir waves, although in this case one needs a causative agent for the Langmuir waves other than the usual <25 keV electrons.

Since the Langmuir waves are usually deemed essential for the emission process, we conclude by reviewing the observational evidence concerning them. The frequency of the

observed spiky electric field structures, such as those in Figure 2.6(a) at 31.1 kHz corresponds satisfactorily to the local plasma frequency based on the measured local electron density. It seems to be inferred that these fields are electrostatic (i.e., longitudinal), since a dipole antenna cannot distinguish polarization. Spin modulation has sometimes shown the fields to be closely aligned with the solar wind magnetic field (Gurnett and Anderson, 1977).

The spiky structure is characteristic. Since the solar wind is sweeping the plasma waves past the spacecraft at $\sim$600 km s^{-1}, and the instrumental time resolution of the electric field is 50 ms, spatial structures smaller than about 30 km cannot be resolved. However, many of the observed Langmuir field spikes do tend to be associated with this size, indicating that even smaller unresolved spatial structures cannot be ruled out.

Gurnett et al. (1980) have grouped together all the 90 electron plasma oscillation events which have been identified to date in conjunction with type III bursts. The data, taken from Helios 1 and 2, Voyager 1 and 2, and IMP-8, is summarized in Figure 2.8. The maximum electric field strength is plotted versus the heliocentric radial distance at which the waves are observed. Although a wide spread is evident at any radius, a power law fit shows a decrease of field with radius, going as $E \approx E_0 R^{-1.4}$, where $E_0 = 0.5$ mV/m. The fall-off

with radius is consistent with the fall-off of the volume emissivity with radius (Figure 2.4), and suggests a causal relationship. The most intense electron plasma oscillations (field strengths from 1-10 mV m^{-1}) are usually detected close to the sun, at heliocentric radial distances less than 0.5 AU. It is noteworthy that the majority of type III bursts occurring near 0.5 AU are not accompanied by measurable Langmuir waves on resolvable scales (Gurnett and Anderson, 1977).

2.2. Microwave Bursts

Microwave bursts are a type of continuum burst, so-called because they extend over a broad range of frequencies from a few tens of gigahertz to several hundred megahertz without any spectral structure (Figure 1.1). Microwave bursts can be classified into impulsive bursts, gradual bursts and microwave type IV bursts (Wild et al., 1963). Impulsive bursts have a time scale of 1-5 minutes and brightness temperatures up to 10^9K. (The brightness temperature of solar radiation is the equivalent temperature which a black body would have which emitted radiation of the same intensity at the same frequency.) Gradual bursts have a time scale of tens of minutes and brightness temperatures up to 10^6K. Microwave type IV bursts have a time scale of 5 minutes to half an hour and brightness temperatures up to 10^9K.

The impulsive microwave bursts are closely correlated with hard X-ray bursts and the intensity profiles usually track

each other, but with some time delay of the order of 1 s for the microwaves when seen with subsecond time resolution. When seen with 20 ms time resolution, the X-rays have 80 ms spikes which are absent in the microwaves as though the microwaves were a smoothed out version of the hard X-rays (Lin et al., 1980). Thus while microwaves and hard X-rays come from related electron populations, they clearly do not come entirely from the same population. This is born out by the VLA maps at 15 and 22.5 GHz with arcsec resolution (Marsh and Hurford, 1980) and the hard X-ray images taken with the Solar Maximum Mission (SMM) with 8" resolution (Hoyng et al., 1981). The microwaves come from the tops of loops and the 16-30 keV X-rays and Hα emission come mostly from the footpoints of the loops.

The accepted radiation mechanism for the microwave bursts is gyrosynchrotron radiation due to electrons with energies greater than about 100 keV spiraling in a magnetic field (Ramaty, 1969; Trulsen and Fejer, 1970). However, occasional fine structure in microwave type IV bursts observed with a time constant of 20 ms have brightness temperatures greater than 10^{13}K (Slottje, 1980) and can only be explained by plasma radiation (Smith and Spicer, 1979). The major problem in interpreting microwave bursts is that several factors affect their intensities and spectra, and we have no independent handle on many of them. The most important of these are non-uniformity of the magnetic field and various low-frequency

absorption mechanisms such as synchrotron self-absorption. Because of these uncertainties, we shall not treat the theory of microwave bursts in detail, but shall consider the related problems of type I and moving type IV bursts in Section 5.

2.3. Type II Bursts

Type II bursts consist of two slow drifting bands near the fundamental and second harmonic of the plasma frequency at meter wavelengths (Figure 1.1). When the drift rate is converted into an effective radial velocity, a velocity in the range 800-2000 km s^{-1} is obtained which was identified with a collisionless magnetohydrodynamic (MHD) shock wave ascending through the corona. This identification was confirmed when a type II burst was observed down to 30 kHz with the IMP-6 satellite (Malitson, Fainberg and Stone, 1973). The last observation was made just before a sudden-commencement geomagnetic storm which is known to occur when an interplanetary shock wave impinges on the magnetosphere of the earth. Several type II bursts have recently been observed below 1.3 MHz with the Voyager spacecraft (Boishot et al., 1980). The relatively frequent occurrence of these bursts at large distances from the sun would favor the hypothesis of shocks propagating parallel to the ambient magnetic field. However, Boishot et al. found that the observed spectral characteristics showed that the source of emission was restricted to only a small portion of the shock which could

well be a region where the magnetic field is locally perpendicular to the shock. Unfortunately, no measurements have been reported to date where the properties of the shock, the energetic electrons and the radio emission have all been measured together with the detail which we have for type III bursts.

It is important for discussing the theory to determine whether radio emission is produced for shock propagation primarily parallel or perpendicular to the ambient magnetic field. For one type II burst at meter wavelengths, Smerd (1970) concluded that a better case could be made for parallel than perpendicular propagation. However, it is also true at meter wavelengths that only a part of the shock emits at any one time since when seen with the Culgoora radioheliograph, one part of the source brightens and fades, and then another part brightens (Wild and Smerd, 1972). This indicates that some special condition must be satisfied for radio emission which may well be related to the mode of propagation of the shock. The brightness temperatures of type II bursts reach about 10^{11}K for both the fundamental and the harmonic in the bright parts of the bursts.

Type II bursts are rich in structure (Wild et al., 1963; Wild and Smerd, 1972). Among the most important of these are: Band-splitting: Each harmonic band is split into two or more components separated by about 10% of the midfrequency

[Fig. 13 of Wild and Smerd (1972)]. These split bands clearly emanate from different spatial locations at 80 MHz which led Smerd, Sheridan and Stewart (1975) to postulate that they arise from emission from ahead of and behind the shock. This is consistent with the fact exemplified in Figure 13 of Wild and Smerd (1972) that detailed spectral features are sometimes duplicated in the two components of a split band.

Herringbone structure: In about 10% of the bursts the harmonic bands consist of a succession of short-lived broad-band elements which have fast frequency drifts of both positive and negative signs like mini-type III bursts. Sometimes these diverge from a narrow-band feature and sometimes this feature is absent.

It can be seen immediately in comparing the observations of type II and type III bursts that we are dealing with a more complex phenomenon with type II bursts. On the other hand, because of their much slower drift, they provide the clearest example of plasma emission at the fundamental and second harmonic and other fine structure clues whose interpretation we shall discuss in Section 4.

2.4. Moving Type IV Bursts

Type IV bursts are a very complex type of continuum radiation which typically occurs after type II bursts in large flares (Fig. 1.1). Some of the radiation must be produced near the plasma frequency due to its high brightness temperature and

some of it must be synchrotron radiation due to the high degree of circular polarization (Wild and Smerd, 1972). A part of the type IV burst moves progressively outward through the corona when viewed with the Culgoora radioheliograph to heights as large as 6 $R_\odot$ with velocities in the range 20-1400 km s^{-1}. This is a moving type IV burst and is often associated with white-light coronal transients indicating the ejection of material (Stewart et al., 1974a,b). Moving type IV bursts have been further classified into three types (Smerd and Dulk, 1971).

Advancing shock front: This appears as a wide irregular arc on the heliograph record some minutes after a type II source has occurred. The arc gradually expands outwards and can be explained as synchrotron radiation at 80 MHz as the source attains a height of $\gtrsim$ 1 $R_\odot$. All varieties of moving type IV bursts have the characteristic of a late first appearance at a height $\gtrsim$ 1 $R_\odot$ at 80 MHz which can sometimes be explained by suppression of synchrotron radiation by the medium (Boishot and Clavelier, 1967).

Expanding magnetic arch: This second variety is due to electrons trapped in a magnetic arch which expands with time. This variety is often associated with an activated filament seen in $H\alpha$. The arch progressively expands at a velocity $\sim$300 km s^{-1} and develops strong circular polarization of opposite senses at its two feet as though electrons are

mirroring near these positions. Often after some expansion as a whole arch, the source condenses into several discrete sources, but still arranged along a loop of increasing dimensions. The emission from the footpoints is best explained as plasma emission for this type.

Ejected plasmoid: The last variety is characterized by uniform radial motion of the source to very great heights occasionally, but more often to 2-3 $R_\odot$. These sources often break up into two sources which are circularly polarized in opposite senses. Although the original interpretation of this type was that a plasma with its own magnetic field is being ejected from the corona, i.e., a plasmoid, the most recent observations with the Culgoora radioheliograph operating at three frequencies (Duncan, Stewart and Nelson, 1981; Duncan, 1981), show that this type is remarkably similar to the expanding arch in a corona whose density has increased by a large factor due to the ejection of a transient. The only difference between these two types is that in the expanding arch the accompanying density enhancement causes a bulging out of the corona whereas in the ejected plasmoid the accompanying density enhancement actually looses its solar attachment and becomes a transient.

The latest observations (Duncan et al., 1981; Duncan, 1981) also show brightness temperatures up to 5×10^{12}K which can only be explained by plasma emission. The observed degree of polarization of up to 100% implies that the emitting

electrons cannot have energies much above 100 keV on the gyrosynchrotron hypothesis. However, 100 keV electrons cannot give gyrosynchrotron brightness temperatures above 10^9K (Duncan, 1981). The observed sense of polarization is o-mode consistent with plasma emission and inconsistent with the x-mode sense expected from gyrosynchrotron emission. It should be noted that until these recent observations plasma emission had been rejected for moving type IV bursts (Dulk, Melrose and Smerd, 1978) because it was thought that electron densities at the heights of moving type IV sources were too small and, on the evidence of one-dimensional interferometers, moving type IV sources showed no dispersion of source position with observing frequency as would be expected for plasma emission. With the Skylab observations of coronal transients, cases were observed with densities as high as 1.5×10^9 cm^{-3} at heights of 3 $R_\odot$ corresponding to a plasma frequency of 270 MHz (Schmahl and Hildner, 1977). The material was confined in threads with steep density gradients so that source dispersion at different frequencies should be different than in the normal corona traversed by a type III burst. The three frequency two-dimensional interferometer observations with the Culgoora heliograph have shown that there is source dispersion at different frequencies in moving type IV sources (Duncan, 1981). Thus we have a case where the use of powerful new

observing techniques has forced a complete rethinking of the interpretation of these bursts. This interpretation for advancing front and ejected plasmoid type sources for which we now have a rich data base will be considered in Section 5.

2.5. Type I Noise Storms

Type I noise storms are the most persistent form of solar activity at meter wavelengths and are not associated with flares, but occur continuously in active regions. They have been reviewed by Elgaroy (1977). The storms consist of type I continuum in the 40-400 MHz range which has a slow rise time, long duration of hours to days and a relative bandwidth of about 100%, and type I bursts which have a rise time ≈0.1 s, a duration of 0.1-10 s and a relative bandwidth of a few percent. The emission of both continuum and bursts is predominately polarized in the sense of the o-mode and often reaches nearly 100%, consistent with fundamental plasma emission. As shown schematically in Figure 1, low-frequency type III storms have approximately the same starting frequency as the lowest frequency of type I emission which lends some support to the hypothesis that the frequency of type I emission is related to the plasma frequency.

However, the directivity properties of type I and type III emission are quite different. As discussed in Section 2.2, type III bursts have broad cones of emission. Observations made from the earth and from a spacecraft at

169 MHz to give a stereo capability have shown that the beam-width of individual type I bursts is less than 25° (Steinberg, Caroubalos and Bougeret, 1974) and sometimes tilted 60° away from the local solar vertical (Bougeret and Steinberg, 1980). The observations of individual type I bursts with high spatial (3.4') and temporal (0.1 s) resolution have shown the existence of bursts whose peak intensity moves during their lifetime which can only be explained by propagation effects that take place very close to the primary source (Bougeret and Steinberg, 1977). The high directivity of individual bursts argues against much isotropic angular scattering of the radiation far from the source. On this basis Bougeret and Steinberg (1977) have developed a model in which the radiation is produced in bunches of overdense fibers and suffers multiple reflections off these fibers. For the model to work they need emission directed along the fibers as would be expected for gyro-synchrotron emission for fibers aligned along the magnetic field.

Heliography has also shown the persistance of a given spatial-temporal shape at the same position which means a broad noise storm center can be divided into a few distinct and fixed sources where bursts of constant characteristics are emitted. This indicates that the burst sources are very well localized and connected with very fixed structures in the corona. In the context of the fiber model, many loops consisting of a number

of fibers with different densities and orientations can make up an active region. Thus close-by sources with different beam orientation would be expected and are sometimes observed (Bougeret and Steinberg, 1980). The noise storm center then consists of many sources that cannot be observed simultaneously from a given direction and the spatial-temporal shape is obtained by strong scattering close to the source inside the fibrous medium. Other observations show that type I sources are located over regions with soft X-ray loop structures (Stewart and Vorpahl, 1977) and it is possible that there are many more loops which are too cool to be observed.

The directivity of type I emission leads to a very marked center-to-limb effect for their observability (Elgaroy, 1977). Since noise storms are associated with loop structures, but can be up to 100% polarized, the emission must be confined to primarily one leg of the loop. Within the fiber bunch model, the center-to-limb variation and degree of polarization is hypothesized to occur as follows (Bougeret and Steinberg, 1980): (i) The radiation is most often oriented in the direction of the fibers with less frequent orientation at large angles. (ii) Propagation transverse to the direction of the fibers results in a depolarization due to multiple reflections. Propagation along the fibers results in very few reflections and little depolarization. (iii) Burst sources are more frequently located in regions where the radiating part of

the arch (bunch of fibers) is close to the solar radial which will produce the observed center-to-limb distribution.

The type I noise storm phenomenon is our last example of a quite complex process which is rich in details which should give many clues for a theory. It is fair to say that no theory to date has been able to explain all the observations. Type I noise storms are related to moving type IV bursts in that they both arise from trapped electron populations, but without the very rapid movement of the traps possible during flare conditions. In fact, type I bursts cluster in "drifting chains" which drift to lower frequency 70% of the time at 1 MHz s^{-1} at 150 MHz which leads to an average velocity of 90 km s^{-1} assuming fundamental plasma emission. At lower frequencies the drift rates and derived speeds are considerably smaller, and consistent with the observed speeds of non-flare-associated rising loops observed in white light (Gosling et al., 1976). Thus we shall consider the theory for type I noise storms along with that for moving type IV bursts in Section 5.

3. THEORY OF TYPE III RADIO BURSTS (RADIO EMISSION FROM ELECTRON STREAMS)

3.1. Overview

We shall only discuss those theories which regard electron-stream-excited Langmuir waves as the source of observed electromagnetic emission, and in which only a small fraction of the Langmuir wave energy is lost by electromagnetic emission processes. The evolution of the Langmuir wave spectrum can therefore be studied independently of any coupling to transverse fields. There are two classes of nonlinear mechanisms which govern the evolution of the Langmuir wave spectrum. "Quasilinear theory" studies the interaction between the waves and the electron stream, and their mutual evolution. "Mode-coupling (or wave-wave interaction) theory" involves coupling between Langmuir waves in different parts of k-space, and includes induced scatter, as well as nonlinear refractive effects. Finally, there may be linear refractive effects due to small density irregularities, which can affect the Langmuir wave spectrum.

3.2. Quasilinear Theory

Quasilinear theory is a statistical theory, in which the ensemble-averaged spectral energy density of Langmuir waves, $P(k)$, grows due to the free energy in a "bump-on-tail" electron distribution function, $F(v)$, which simultaneously evolves because of diffusion in velocity space as electron orbits are

perturbed by the Langmuir waves. Most theories are one-dimensional. For a homogeneous beam, a plateau eventually forms in velocity space, and Langmuir wave growth stops. (On a much longer time scale, both the beam and the waves will thermalize, due to collisions.)

However, we know from observation (Figs. 2.6, 2.7) that the electron streams associated with type III bursts are not spatially homogeneous. Due to velocity dispersion, the fast electrons arrive before the slow ones [Fig. 2.6(b)]. As shown in Figure 2.7, the peak of the "bump-on-tail" distribution moves from higher to lower speeds. Waves emitted at early times with phase velocities matched to electron velocities, v, for which the "bump", F(v) has positive slope should therefore be reabsorbed at later times, when the phase velocities correspond to a (displaced) bump with negative slope. In this way, the stream can propagate over long distances.

"Inhomogeneous" quasilinear theory is required to treat the process quantitatively. Early analytical predictions by Ryutov and Sagdeev (1970) have been developed and confirmed in the context of type III burst streams (Zheleznyakov and Zaitsev, 1970a,b; Zaitsev et al., 1974; Grognard, 1975). The most complete calculations require extensive numerical work (Takakura and Shibahashi, 1976; Magelssen and Smith, 1977; Grognard, 1980). The 1-D inhomogeneous quasilinear equations solved by Magelssen and Smith had the following form:

$$\frac{\partial P}{\partial t} = \left[a\, v^2\, \frac{\partial F}{\partial v} - \gamma_b\right] P + a'\, vF + \beta \ , \qquad (3.2.1a)$$

$$\frac{\partial F}{\partial t} + \frac{\partial F}{\partial x} = -\tau\, F + b\, \left[\frac{\partial F}{\partial v} + \frac{\partial}{\partial v}\, \left(\frac{P}{v}\, \frac{\partial F}{\partial v}\right)\right] \ , \qquad (3.2.1b)$$

where a, a' and b are constants, γ_b and β represent wave damping and spontaneous emission by the background plasma, and τ represents (slow) collisional relaxation of the beam. In (3.2.1a) P(k) is driven unstable at wavenumbers, k where the slope of the bump, $\partial F/\partial v$, is positive, and where the Cerenkov condition, $v = \omega_p/k$, is satisfied. Spontaneous emission is included in the a' term. In (3.2.1b) the advective term, $v\, \partial F/\partial x$, is the essential new feature in the inhomogeneous theory. Equations (3.2.1a,b) were solved, subject to the boundary condition of an assumed stream with $F \propto v^{-5}$ $\exp\left(-(t-t_0)^2/T^2\right)$, generated at the injection point, low in the solar corona. Typically, t_0 and T were chosen on the order of seconds. In Figure 3.1, we see a time-ordered sequence of profiles of F and of P, at a distance 2×10^9 m from the injection point. Both velocity dispersion and reabsorption are evident, as well as plateau formation.

A central result of any nonlinear calculation is the predicted total energy density in Langmuir waves at a given spatial point. We define the dimensionless Langmuir energy density as

$$W \equiv \frac{\langle |E|^2 \rangle}{4\pi\, n_e\, k_B\, T_e} = \int \frac{dk}{2\pi}\, \frac{P(k)}{n_e\, k_B\, T_e} \ , \qquad (3.2.2)$$

where n_e is the electron density and $k_B T_e$ the electron thermal energy. For the quasilinear calculations the peak energy density is, $W \approx 10^{-5}$ typically. Grognard (1980) used the one-dimensional distribution function found by Lin et al. (Fig. 2.7) as a boundary condition for integrating the quasilinear equations forward, to a spatial point downstream. An initially low level of waves was found numerically to grow to $W \approx 10^{-5}$, in agreement with the peak Langmuir electric fields of several mV/m measured by Lin.

Finally, it is worth remarking that inhomogeneous quasilinear theory predicts, at a given spatial point (and thus a given plasma frequency) a temporal build-up of W^2 to a maximum and then a temporal relaxation which is in accord with the temporal emission profiles in Figure 2.3. This was first noted by Zaitsev et al. (1972), and confirmed by Smith and Magelsson. It is significant because the theory of second harmonic emissions gives volume emissivities quadratic in the Langmuir wave spectral energy density (see Section 3.5). If the emission is assumed to be fundamental, a somewhat less adequate fit is still possible (Zaitsev et al., 1972).

3.3. Induced Scatter Off Ions

Quasilinear phenomena and the process of induced Langmuir scatter off the polarization clouds of ions (or off ion-acoustic waves, when $T_e \gg T_i$) together comprise the subject matter of "weak turbulence theory", provided the

scatter is treated statistically (using the random phase approximation). Kaplan and Tsytovich (1967, 1973) considered induced scatter off ions independently of quasilinear theory, as a stabilization mechanism which removes Langmuir wave energy from resonance with the beam. Zheleznyakov and Zaitsev (1970a) treated induced scatter off ions together with quasilinear theory for the lower corona (100 MHz < f_p < 200 MHz), and concluded that the former was negligible. Later work seemed to support this conclusion, by showing that the energy density in Langmuir waves had to be comparable to the energy in the electron stream for induced scatter to become important (Smith and Fung, 1971; Heyvaerts and de Genouillac, 1974).

More recent estimates (Smith, 1977), based on spacecraft observations at lower frequencies, show that it cannot be neglected in comparison with quasilinear effects for the values $W \approx 10^{-5}$ measured in intense bursts at 0.45 AU. It is estimated that the time for the scattered wave energy to equal the beam-resonant wave energy is about 40 s, which is an order of magnitude shorter than the duration of the Langmuir waves. Induced scatter is therefore a fast process.

There is some difference of opinion over whether induced scatter is principally a 1-D or a 3-D process. In 2-D numerical calculations of induced scatter off ion-acoustic quasimodes, it is found to occur as a 1-D backward or forward

scatter (Bardwell and Goldman, 1976; Nicholson and Goldman, 1978; Hafizi, Weatherall, Goldman and Nicholson, 1981). Other authors claim it is essentially 3-D (Heyvaerts et al., 1974; Perkins et al., 1974).

If one considers the 1-D scatter in the dimension defined by the wave vector, $\underline{k}_0$, of a beam-resonant "pump" Langmuir wave, then the scattered wave-vector is determined from the kinematical condition $\omega_L(\underline{k}_0) = \omega_L(\underline{k}_s) + v_i|\underline{k}_0-\underline{k}_s|$, where $\omega_L(k) = (\omega_p^2+3v_e^2k^2)^{1/2}$ is the Langmuir wave dispersion relation and v_i the ion thermal velocity. This leads to a scattered Langmuir wave vector, $k_s/k_D = \alpha - k_0/k_D$, where $\alpha = (2/3)(m/M)^{1/2} = 1.55 \times 10^{-2}$, in a plasma with equal electron and ion temperature, and k_D is the Debye wave number, $(4\pi ne^2/k_BTe)^{1/2}$. Since the beam-resonant wave number is $k_0/k_D = v_e/v_t$, the character of the scatter depends on the size of v_e/v_t relative to α. If it is assumed that $v_e/v_t \gg \alpha$, as in most of the early work near 100 MHz, then the scattering is in the backward direction until the scattered mode builds up enough energy to act as a pump for a secondary scatter into the forward direction. During each scatter, the wave number is reduced by α (see Nicholson and Goldman, 1978 for a graphic illustration) until the cascade of multiple scatterings builds up a distribution of Langmuir waves in both directions, between $\underline{k}_0$ and $-\underline{k}_0$. In the 3-D version

of this, an isotropic distribution is created. However, the measured beam near 1 AU (Fig. 2.7) has the property that k_0/k_p is of the same order as α, so that only a single scatter should occur, bringing Langmuir waves to essentially zero wave number. In preliminary calculations, using the data in Figure 2.7, Grognard (1981) has studied quasilinear and induced scatter effects near 1 AU simultaneously, and observed an important role played by the latter, leading to a build-up of scattered energy at wave numbers much less than beam-resonant wave numbers. The resulting spectrum may be unstable to modulational instability and spatial self-focusing as discussed in the next section.

3.4. Wave-wave Effects of the Nonlinear Refractive and Self-focusing Variety

The fundamental equations underlying most discussions of this wider class of wave-wave interactions is the pair of beam-driven Zakharov equations for the slowly varying complex envelope, $\underline{E}(\underline{r},t)$ of electrostatic electric field oscillations near the plasma frequency [of form $\underline{E}(\underline{r},t) = \mathrm{Re}\ \underline{E} \exp(-i\omega_p t)$], and the slowly-varying density perturbation $\delta n_2(\underline{r},t)$ which is second order in $\underline{E}$. With time in units of ω_p^{-1}, and distances in units of $\sqrt{3}\ k_D^{-1}$, these equations assume the following general form (Zakharov, 1972; Nicholson et al., 1978; Goldman et al., 1980a)

$$i\,\partial_t\,\underline{E} + 1/2\,\nabla^2\,\underline{E} - \frac{\delta n_2}{2n_0}\,\underline{E} - i\,\hat{\gamma}\,\underline{E} = 0\,, \qquad (3.4.1a)$$

$$[\partial_\tau^2 + \hat{\nu}_i\,\partial_t - c_i^2\,\nabla^2]\,\delta n_2 = \frac{n}{2\pi\,M\,\omega_p^2}\,\nabla^2\,|E|^2\,. \qquad (3.4.1b)$$

In the first equation, the term $\delta n_2 \underline{E}$ contains nonlinear refractive effects arising from density changes, δn_2. In the second equation, δn_2 is driven by the divergence of the pondermotive force, $-\underline{\nabla}\,e^2\,|\underline{E}|^2 4m\,\omega_p^{-2}$, and responds through the linear ion-acoustic (quasi-) mode operator in square brackets on the left. The velocity is the ion (sound) speed in these special units. The term $\hat{\gamma}E$ in the first equation has the spatial Fourier transform $\gamma_k\,\underline{E}_k$, where γ_k is the growth rate of Langmuir waves due to an idealized electron stream, with no velocity dispersion, which propagates unaffected by the waves. The growth rate γ_k is a maximum of order $(\pi/8e)^{1/2}$ $(n_b/n_0)(v_b/\Delta v)^2$ in a small region of k-space near $\underline{k}_0 = \omega_p\,\hat{\underline{v}}_b/v_b$, where resonant waves are driven by the beam. The term $\hat{\underline{\nu}}_i\,\delta n_2$ in the second equation has the spatial Fourier transorm $\nu_{ik}\,\delta n_k$, where ν_{ik} is the damping rate of ion-acoustic waves, usually assumed to be of the order of their frequency, $c_i k$, because of heavy ion Landau damping of ion-acoustic (quasi-) modes in a plasma with $T_e = T_i$.

The Zakharov equations (3.4.1) are dynamical, rather than statistical in nature, unlike the quasilinear equations

(3.2.1). One solves for the amplitude and phase of the electric field envelope $\underline{E}(\underline{r},t)$ or its transform, $\underline{E}(\underline{k},t)$, rather than for a spectral energy density, $P(k) = \int d^3(\underline{r}_1-\underline{r}_2)$ $\langle \underline{E}(\underline{r}_1)\cdot\underline{E}(\underline{r}_2)\rangle \exp i\underline{k}\cdot(\underline{r}_1-\underline{r}_2)$, where $\langle\rangle$ denotes an ensemble average. The Zakharov equations do not allow for nonlinear modifications of the beam distribution function, whereas the pure quasilinear equations do not allow for any wave-wave interactions. Moreover, the Zakharov equations are three-dimensional, and contain induced scatter off ions, as well as important effects such as self-focusing which require at least two spatial dimensions (Goldman and Nicholson, 1978b; Goldman et al., 1980b; Hafizi et al., 1981), whereas the quasilinear equations are usually solved in one dimension.

In Equation (3.4.1a) it is assumed that the transverse electric field and its sources are much smaller than the longitudinal field and its sources. With this approximation, the coupled equations have been solved numerically in a two-dimensional cell with periodic boundary conditions (Nicholson et al., 1978; Goldman et al., 1981). The most recent results, for parameters appropriate to 0.5 AU, are shown in Figure 3.2 (Hafizi et al., 1981) in which contours of equal $|\underline{E}_{\underline{k}}|$ are plotted in k-space. Initially all modes are at a low level, and randomly phased with respect to one another. The beam-resonant or "pump" modes in the rectangle grow up temporally, to a level $W_p = 10^{-5}$. At time t_1, energy is

beginning to go to lower wavenumbers [Fig. 3.2(a)]. At time t_2, the three contours labelled by 2 in Figure 3.2(b) represent linear wave instabilities pumped by the beam-resonant modes. The two contours off the axis represent a modulational instability, in the geometry predicted by Bardwell and Goldman (1976). This differs from the one-dimensional geometry predicted by Papadopoulos et al. (1974). The contour near the origin represents induced scatter off ions, which is contained in the dynamical Zakharov equations as well as in weak turbulence theory. At the slightly later time, t_3, shown in Figure 3.2(c), there is very little Langmuir energy left in resonance with the pump, and the rate of energy injection into all modes has therefore slowed considerably. As viewed in coordinate space around this time, Langmuir wave packets are seen to begin to collapse spatially to smaller dimensions. The background solar magnetic field may be incorporated into the calculation, and tends to make the wave packets slightly pancake-shaped at the early stage of collapse (Goldman et al., 1981), but does not change the scenario significantly.

The physical origin of this spatial self-focusing is as follows: Pondermotive force causes a local reduction in density and increase in the "index of refraction" seen by the Langmuir waves. In two or more dimensions (Goldman and Nicholson, 1978; Goldman et al., 1980b) this refraction cannot be compensated by dispersion, and the packet collapses

unstably, until it is dissipated by background electrons at a scale size of several Debye lengths, or broken up by scattering off density cavities.

Unfortunately, the Zakharov equations cannot be solved accurately for times much later than t_3, so it is not known how long the collapse continues. Presumably a steady state evolves, and the electromagnetic emission may come from either the small scale or larger scale structures, or both. Kruchina et al. (1980) argue heuristically that this steady state is dominated by Langmuir scatter off density cavities. They construct a crude statistical theory in which field correlation times are controlled by phase shifts associated with this scatter. They argue that the large scale structures are principally responsible for the emission, and derive emissivities which are consistent with the data of Figure 2.4.

Goldman et al. (1980a) have calculated the emission from a single collapsing (self-similar) wave packet in the late stage, when small spatial scales are reached. However, a volume emissivity requires, in addition, a knowledge of the density of such collapsing packets, which cannot be found reliably without a knowledge of the steady state.

The study of the implications of the Zakharov equations for the Langmuir turbulence associated with type III bursts has been frought with difficulties. It was originally thought that beam-resonant wave packets collapsed directly, before any

induced-scatter off ions could occur (Nicholson et al., 1978; Goldman and Nicholson, 1978). Other authors also neglected induced scatter off ions, in heuristic 1-D statistical theories in which direct modulational instability of the beam modes led to a transfer of energy to higher wavenumbers and eventual stabilization to a steady state (Smith et al., 1979; Goldstein et al., 1979; for a more rigorous theory of 1-D strong Langmuir turbulence, also see DuBois and Rose, 1981). Such 1-D theories probably do not describe the rapid collapse stage properly (Rowland et al., 1981; Hafizi et al., 1981) and the one-dimensional nature of the modulational instability has been criticized. However, in the context of the type III problem, all of these attempts give peak energy densities between $W = 10^{-5}$ and $W = 10^{-4}$, and all quickly remove Langmuir energy density from resonance with the beam. This is because the thresholds for induced scatter off ions, modulational instability and direct collapse are all very close to one another, and all involve relatively fast transfers of energy in k-space, compared to the time scale for quasilinear plateau formation.

The "spiky" spectrum of Langmuir waves measured between 0.5 AU to 1 AU (Figure 2.6) cannot be taken as evidence for collapsed wave packets, because the minimum resolvable distance of $\sim$25 km is much larger than the size of a collapsed packet of ten Debye lengths ($\sim$50 meters) or even the wavelength of the

beam-resonant Langmuir modes ($\sim$3 km). It is possible the small k condensate of Figure 3.2(c) is observable, but we do not know theoretically what fraction of the energy of an eventual steady state Langmuir spectrum lies at such small wavenumbers.

In Figure 2.8, the line corresponding to $W = 4 \times 10^{-5}$ lies near the upper limit of the measured Langmuir field strengths. It is important to note that this value of W, although common to most theoretical treatments, is associated with much shorter scale length Langmuir turbulence than the measured fields with scale lengths $\gtrsim$25 km.

3.5. Second Harmonic Emission From Langmuir Waves

There are no plausible mechanisms for production of second harmonic emission other than the coalescence of two Langmuir waves, first proposed by Ginzburg and Zheleznyakov (1958). Even this requires the beam-resonant Langmuir modes to undergo spectral modification, by wave-wave interaction or by scattering off density irregularities. The reason has to do with the necessary kinematical matching restriction, $\omega_L(\underline{k}_1) + \omega_L(\underline{k}_2) = (\omega_p^2 + c^2 k_T^2)^{1/2}$. Since the two Langmuir frequencies are very close to the plasma frequency, the transverse wavenumber of the harmonics emission must be $k_T \approx \sqrt{3}\,\omega_p/c$, regardless of the Langmuir wave-vectors $\underline{k}_1$, $\underline{k}_2$. If we take the magnitude of these wave-vectors to be of the order ω_p/v_b, assuming them to be resonant with the beam, then the momentum matching condition, $\underline{k}_1 + \underline{k}_2 = \underline{k}_T$, tells us that we

must have $v_b \approx (2/\sqrt{3})\ c$, which is impossible. The stream velocity is known to be c/2 or less, so the wave-vectors of the beam-resonant waves are too large to add up properly. Induced scatter off ions into the backward direction may lead to a "correct" spectrum for second harmonic emissions. Also, the real-space collapse of this condensate may eventually create a broad spectrum of backward and forward waves which would be kinematically suitable for second harmonic emission.

The current which produces second harmonic emission is second order in the Langmuir field: $j_2 \sim \delta n_1\ E$ where $\delta n_1 \propto \underline{\nabla} \cdot \underline{E}$, by Poisson's equation. The emissivity is proportional to $|j_2|^2$ and so depends on E to the fourth power. In weak turbulence statistical theories of the volume emissivity, the random phase appropriation is employed and the emissivity goes as P^2. This may not be the case, however, for statistical theories of strong turbulence even with random phases. (Kruchina et al., 1981; Goldman et al., 1980; Papadopoulos et al., 1978). Moreover, there can be important phase effects, in the dynamical evolution of the Langmuir fields, which are neglected if collapse plays a role (Hafizi and Goldman, 1981).

There are a number of different estimates for the dependence on W of the volume emissivity at the second harmonic. Smith's (1977) estimate, combining rigorous inhomogeneous quasilinear theory results with heuristic arguments concerning induced scatter off ions gives a volume

emissivity of $J_{2\omega_p} = 10^{-13}\ E^4/\sqrt{n}$ watts m^{-3} sr^{-1}. which is large enough (Gurnett et al., 1980) to account for most of the observations at 1 AU (Fig. 2.7). However his treatment of the scatter is very heuristic and Smith's own claim that the induced scatter is very fast, and goes towards small forward wave numbers during the rise of the burst suggest that the estimate may not be self-consistent. Grognard's preliminary self-consistent calculations of the two effects together, shows the Langmuir spectrum builds to a large "condensate" at small k. This spectrum would not radiate at the second harmonic at all because the kinematics cannot be satisfied. Moreover, the spectrum seems to be above the collapse threshold, and would therefore be expected to spread to higher wave numbers.

Papadopoulos et al.'s (1974) estimate assumes a 1-D isotropic spectrum peaked at $k \sim 0.1\ k_D$, where they claim the modulational instability has the maximum growth rate. Gurnett et al. (1980) obtain from this the volume emissivity $J_{2\omega_p} = 5.8 \times 10^{-15}\ (T/T_o)^{3/2} E^4/\sqrt{n}$ watts/m^3 sr, where T_o is the electron temperature at the earth. This accounts for many fewer of the events observed at 1 AU. Both the one-dimensional nature of this calculation, and the related failure to describe collapse have been criticized (Goldman et al., 1980a; Hafizi et al., 1981; Rowland, et al., 1981). Gurnett et al. (1980), using their measured radial variation of the emissivity, however, show that both of the above estimates are consistent

with the measured radial variation of the Langmuir field (although we must point out once again the disparity of theoretical and measured Langmuir wave scale sizes).

Papadopoulos and Freund (1978) calculate the emission from stationary solitons, assumed to arise from a balance of growth in beam modes, γ_o, against a transfer rate γ_{NL} associated with 1-D modulational instability. They find the volume emissivity for second harmonic generation is proportional to the first power of W rather than the second. In addition, they argue that they can account for the two regimes of dependence of the emissivity on the electron flux J_E, observed by Fitzenreiter et al. (1976), and shown in Figure 2.5. The argument is nominally based on a transition between two forms of the modulational instability, the subsonic [in which the first two terms on the left in Equation (3.4.1b) are negligible] and the supersonic (in which they are dominant). We believe this argument to be unconvincing for a number of reasons. The most serious objection is that it requires a beam to background density ratio, $n_b/n_e \approx 3 \times 10^{-4}$, which is three orders of magnitude higher than is usually assumed reasonable. In addition, it is difficult to justify the stable solitons they assume, or the closely packed density of such solitons (Goldman et al., 1980a).

Goldman et al. (1980a) calculate the second harmonic (and fundamental) emissivity from a single collapsing soliton,

and find both an upper limit which is quadratic in W, and a lower estimate, based on a supersonic self-similar solution, which is independent of W. A volume emissivity is then obtained from a crude statistical model which gives the density of solitons by balancing the power flow into beam modes against the power transfer to collapsing solitons. However, this model contains an undetermined parameter, F, relating to the lack of knowledge concerning the amount of Langmuir energy in resonance with the beam. The parameter, F, cannot be determined without the (2-D) steady-state strongly turbulent spectrum of Langmuir waves. At present, this spectrum has not been determined numerically. In addition, the assumption was made that the collapse was direct, i.e., that it proceeded from wave packets whose size and shape was determined by the width and location in k-space of the beam-resonant mode spectrum. The latest, more detailed, results [Figs. 3.2(a)-(c)] show the collapse is not direct, but proceeds from a condensate near zero wave number, which forms after induced scatter off ions has occurred (Hafizi et al., 1981). This will affect both the dynamical and statistical assumptions which enter into the calculations of emission from collapsing solitons, particularly because the beam-modes are severely depleted up to the latest times which can be followed (Fig. 3.2).

Kruchina et al. (1981) consider the emissions from a strongly turbulent Langmuir state in which Langmuir wave

packets are nonlinearly phase de-correlated due to scatter off density cavities. They find an emisnivity for second harmonic emission which is linear in W, and also claim good agreement with the data of Figure 2.4. Their model, however, is one-dimensional and based on a scenario for steady state Langmuir turbulence which has never been obtained numerically even in 1-D for the streams associated with type III bursts (although there is some evidence for such a 1-D spectrum in laser-driven plasmas). In addition, one might expect much lower cross-sections for scatter of wave-packets from density cavities in two or three dimensions.

These tneoretical studies usually interpret local low-frequency type III emissions as second harmonic, in which case, none are able to account for the characteristic ten- to twenty-minute delay between the onset of the local emission and the onset of both the observed Langmuir waves and the positive-slopes part of the parallel electron distribution function. Since Lin et al. (1981) are now calling into question the interpretation of the low frequency emissions as second harmonic, more careful consideration ought to be given to the predictions from strong turbulence theory of fundamental emission at low frequencies.

3.6. Fundamental Emission From Langmuir Waves

There is no way a Langmuir wave can convert into fundamental radiation near the plasma frequency without some

agent to take up momentum. This follows from the frequency and momentum conservation laws. In the presence of local density gradients, the inverse scale length of the gradient can act as the required momentum, and so-called direct emission can occur. This effect cannot be dismissed out of hand (Melrose, 1981, 1980b).

In the more traditional scenario, the extra momentum is supplied by ions (through their surrounding polarization clouds). This process was first proposed by Ginzberg and Zheleznyakov (1958, 1959). It has been shown (Smith, 1970; Melrose, 1977) that unless this conversion off ions is induced, there is a problem in accounting quantitatively for fundamental emission at high frequencies.

Another possibility is that the conversion is off very low-frequency waves, which may be present at turbulent levels. Melrose (1980b) has considered this process in connection with emission above 60 MHz, although no theory for the Langmuir turbulence is provided. If the low-frequency waves have W_{low} greater than about 10^{-9}, he finds the fundamental can be as bright as the Langmuir waves. Melrose (1980b) also considers the usual coalescence process for second harmonic emission. He shows that the fundamental, second harmonic and Langmuir waves can all have the same brightness temperature (in agreement with observation) provided that the Langmuir wave brightness temperature is as large as 10^{15}°K. The argument is advanced

that the observed brightness temperatures (of 10^{12}°K for f_p > 40 MHz) should be much less than the actual brightness temperature of the emission if the actual size of the source is much less than the observed size (due, for example, to coronal scattering, or to clumpy Langmuir waves).

At lower frequencies, there has been less work done on fundamental emission. Kruchina et al. (1981) find that the fundamental emissivity goes as W^2 in their version of strong turbulence theory. At 0.5 AU they find equal emissivity for fundamental and harmonic emission, and general agreement with the data of Figure 2.4. Goldman et al. (1980) also find comparable fundamental and harmonic emission from a self-similar supersonic collapsing soliton.

3.7. Density Irregularities and Ion-Acoustic Waves

The existence and significance of static density irregularities and low frequency wavelike density structures, in relation to type III bursts, can no longer be ignored. Scattering and ducting of high frequency emissions off density irregularities have been invoked to explain the differences between apparent and true source sizes and heights in the lower corona (Section 2.1.1). Density irregularities can play a role in fundamental emission, either by allowing direct emission (Melrose, 1980b), or by reducing absorption in induced conversion off ions (Smith and Riddle, 1975; Melrose, 1980b). Irregularities have also been called upon to explain the 1.85

ratio of harmonic to fundamental as due to truncation of the lowest fundamental frequencies due to reflection off irregular density peaks.

Spacecraft proton density measurements show considerable variation in the average density with position and time (Gurnett et al., 1978a). There is also direct evidence for density irregularities from interplanetary scintillations in the emission from radio stars. Coles and Harmon (1978) have studied the spectrum of scintillations at distances $\gtrsim$0.5 AU from the sun. It has been shown that the amplitude, $\delta n/n$, of density irregularities of size between 50 km and 200 km is $\delta n/n \approx 10^{-3}$, to within an order of magnitude. Smith and Sime (1979) have found that linear beam-driven Langmuir rays in such a (weakly) clumpy plasma are strongly refracted into a random pattern of intense and weak spots. The random pattern of Langmuir intensity is consistent with the typically spiky Langmuir fields found by all observers (see Fig. 2.8) and provides a better explanation than the collapse scenario, because the spatial scales are correct. In addition, the isotropization of Langmuir rays as they wander through the density irregularities may help enable the kinematical condition for second harmonic emission to be satisfied.

Ion-acoustic turbulence has been found experimentally to be a permanent feature of the solar wind (Gurnett et al., 1979). Low frequency energy densities $W_{low} = E^2/4\pi n\theta$ of the

order of 10^{-8} are not common between 0.6 AU and 1 AU. This corresponds to values of $\delta n/n = (k_{De}/k)\, W_{low}^{1/2}$ which can be as large as 10^{-4} or more, if the waves are assumed to be ion-acoustic. The observed high levels of ion-acoustic turbulence would also be sufficient to enable Melrose's process of fundamental amplification by induced conversion of Langmuir waves off ion-acoustic waves to occur. The analogue of this process, induced scatter of Langmuir waves off ion-acoustic waves into other Langmuir waves, should be equally fast and efficient. [Ion acoustic turbulence in the vicinity of Jupiter's bow shock has been found by Gurnett et al. (1981), and seems to have a profound effect on Langmuir turbulence, shifting it up to high wave numbers by a cascade of scatters.] The effect of ion-acoustic turbulence on collapse has not been considered, but inhibition would not be surprising. Finally, we should mention that there are processes which enable electron streams to radiate fundamental emission directly, in the presence of ion-acoustic turbulence, without the need for any excitation of Langmuir waves at all (Nambu, 1981).

4. RADIO EMISSION FROM SHOCK WAVES AND CURRENT SHEETS

We move from the relatively simple case of a low density beam which acts as a nonperturbing exciting agent to shock waves which act as a perturbing exciting agent. A perpendicular magnetosonic collisionless shock wave (defined in Section 4.1) is of necessity a current sheet because the magnetic field changes across the shock and its curl gives rise to a current. A stationary current sheet in the corona can always be thought of as two colliding and thus stationary shock waves of this type. We shall not treat current sheets in detail, but having noted the relation between current sheets and shock waves, it should be clear how the results for shock waves could be extended to current sheets. Some results on radio emission from current sheets are given in Smith and Spicer (1979).

4.1. Shock Configuration

By a collisionless shock wave we mean a propagating transition layer that causes a change of state in which the primary dissipation mechanism is not Coulomb collisions between particles. The shock is at least on the average stationary in time in its rest frame. Since ordinary Coulomb collisions are not important, the time scales of all relevant processes must be much less than the collision time. The change in state which occurs when the shock traverses a plasma comes from the collective interaction between particles and electric and

magnetic fields. The fields can be of two kinds: 1. constant in time, produced by charge separation, currents, or external sources, 2. fluctuating in time, produced by plasma instabilities. The first case is called laminar and the second turbulent. The turbulence can be either microturbulence generated by short-wavelength instabilities inside a laminar shock layer or large scale turbulence associated with the dominant mode of the shock structure. Collisionless shock waves have been treated in detail by Tidman and Krall (1971). Hereafter only shock waves of this type will be considered.

The main paramaters required to describe the state of a shock wave are the Alfvén Mach number,

$$M_A = \frac{u}{V_A} \qquad (4.1.1)$$

where u is the shock speed, and the angle between the unshocked or upstream magnetic field B and u. We are restricting the discussion to a low beta plasma where $\beta = 8\pi n_1 K(T_{e1}+T_{i1})/B_1^2$, is the ratio of plasma to magnetic pressure. Extension to the case of arbitrary β can be found in Tidman and Krall. Subscripts 1 refer to upstream variables and subscripts 2 refer to downstream or shocked variables. Shocks with $\psi_1 = 0$ and 90° are called parallel and perpendicular shocks, repectively. Shocks with other values of ψ_1 are called oblique shocks.

The important property of shock waves for our purposes is the manner in which they can lead to the generation of

Langmuir waves. This can occur in two ways: 1. A relative drift of two distinct groups of electrons with a drift velocity $v_D > (3)^{1/2} v_e$ occurs in the shock structure. 2. The shock accelerates electrons to velocities much larger than v_e in the ambient plasma upstream or downstream from the shock. The resulting beams of electrons produce Langmuir waves upstream and/or downstream from the shock. We note in passing that it is insufficient to heat electrons in the shock and let them interact with the cooler electrons of the ambient corona. As shown by Melrose (1980), no nonrelativistic isotropic distribution of electrons can lead to plasma waves with an effective temperature greater than 3×10^9K. Since the brightness temperature of type II emission reaches 10^{11}K, this type of process, which was proposed by Krall and Smith (1975) and Zaitsev (1977), can be dismissed. Heating in the shock plus a selection mechanism which only allows fast electrons to escape along field lines as in Smith (1971) is a viable mechanism because a beam is formed. Since fundamental and second harmonic emission in type II bursts are often of comparable brightness temperature, the fundamental radiation must be amplified (cf. Section 4.3). The amplication requires regions of thickness much larger than the thicknesses of any of the above shocks. These regions can occur upstream or downstream of the shock if the shock can either: 1. selectively accelerate electrons to velocities greater than $(3)^{1/2} v_e$

in these regions so that beams are formed, 2. inject beams into these regions by heating electrons together with a selection mechanism.

It might be thought that Langmuir waves excited in the shock could propagate upstream or downstream from the shock. However, the frequencies of these waves in the upstream or downstream plasma are always considerably less than the local plasma frequency ω_{pe} and they can neither propagate nor lead to radiation which can propagate. This was shown by Smith and Krall (1974) for perpendicular shocks and can easily be generalized to oblique shocks which are rarefaction shocks (cf. Tidman and Krall, 1971). Parallel shocks do not give rise to drifts v_D approaching v_e (Zaitsev and Ledenev, 1976) and thus there is no possibility of exciting Langmuir waves in the shock itself. The physical reason is that most of the current in the shock is carried by electrons and Langmuir waves exist in the frame of these electrons. The Langmuir waves can be excited by an ion beam or an electron beam associated with a small group of suprathermal electrons associated with the VB drift (Pesses et al., 1981, Section 4.2). In either case for Langmuir waves to be excited the effective velocity of the current v_D must be a significant fraction of v_e. Thus in the coordinate system of Figure 4.1, the wavenumber k_y of the excited plasma waves must be of order ω_p/v_e and $k_y v_D$ must be a significant fraction of ω_p. The frequency of the

waves in the rest frame of the ions or shock frame, is $\omega_p' - k_y v_D \approx \omega_p - \delta\omega_p \approx \alpha\omega_p$, where ω_p' is the frequency of plasma waves in the current carrying electrons rest frame, δ is a number of order unity and α is a number of order zero. Thus these waves are of low frequency in the frame of the upstream or downstream plasma and cannot propagate.

Zaitsev (1977) proposed that the frequencies of these waves could be boosted by induced scattering on electrons moving with velocities $v_s > v_e$. The problem with this process is that the amplification distances required are much larger than the thicknesses of any of the above shocks for any energy density in Langmuir waves $W_p < nKT_e$ (Smith, 1972c). Zaitsev does not consider whether the Langmuir waves can be amplified, but only if they can be isotropized. The formulae for isotropizing the Langmuir waves which are low frequency in the ion frame and for amplifying Langmuir waves which have been scattered to high frequency in this frame are quite different. In fact a significant energy density in Langmuir waves scattered to high frequency in the ion frame does not occur. This means that plasma emission from shock waves must be associated with the acceleration or injection of beams of electrons in the upstream or downstream plasma.

As a prelude to discussing beam formation properties in Section 4.2, we state the thicknesses of fast-mode magnetosonic shocks. Fast-mode shocks are shocks in which the basic flow is

decelerated and $B_{t2} > B_{t1}$ where B_t refers to the transverse component of the magnetic field (Tidman and Krall, 1971). These are the only shocks capable of effectively accelerating electrons. A laminar perpendicular shock has a characteristic thickness of c/ω_{pe}. When this shock becomes turbulent for Alfvén Mach numbers $M_A \gtrsim 2$ the width increases to $\approx 10\ c/\omega_p$ (Smith, 1971). High Alfvén Mach number laminar oblique shocks also have a width of several c/ω_{pe} while for low Alfvén Mach numbers ($M_A \lesssim 2$) the characteristic thickness is c/ω_{pi} where ω_p is the ion plasma frequency (Tidman and Krall, 1971). Turbulent oblique shocks have not been studied in detail. For typical coronal parameters ($n = 10^8\ cm^{-3}$) $c/\omega_{pi} = 2.3 \times 10^3$ cm which shows how thin even the thickest of these structures are. We do not consider parallel shocks because possibilities for producing beams with them are poor.

4.2. Generation of Electron Streams by Shock Waves

Shock Waves

There are two main possibilities for this process: 1. heating of electrons in the shock coupled with a selection mechanism, 2. multiple encounters of an electron with the shock causing direct acceleration. An example of the first process was given by Smith (1972b). An almost perpendicular turbulent shock with $2.0 \lesssim M_A \lesssim 2.9$ heats electrons preferentially through the ion-acoustic instability. For $86° < \psi_1 \leq 90°$ only fast electrons can run upstream of the shock and form a beam.

The potential drop associated with the gradient of the electric field E_y in Figure 4.1 was not taken into account in these calculations and they need to be refined. While this will change the selection criterion somewhat because the electrons have to climb up a potential hill, it will still remain a viable mechanism. However, the quite restrictive range of ψ_1 required is unlikely to be fulfilled over large areas of the shock and we proceed to examine the possibilities for acceleration in the upstream or downstream plasma.

A large amount of work has been done in the past few years on acceleration in interplanetary and interstellar shock waves (Armstrong et al., 1977; Axford et al., 1977; Bell, 1978, Pesses et al., 1981). It is the last of the referenced papers and extensions in progress (Pesses, private communication) which are the main basis of our review. For fast mode non-parallel ($\psi \neq 0$) magnetosonic shocks the incoming plasma is decelerated and heated in the shock front over a distance of a few thermal ion gyroradii which is comparable to the c/ω_{pi} estimate at the end of Section 4.1. The large gradients in $|\underset{\sim}{B}|$ and the plasma bulk velocity combined with the induced electric field $\underset{\sim}{E}_y$ that exists in the shock rest frame (Fig. 4.1.1) are responsible for the acceleration of energetic electrons. By energetic we mean electrons whose kinetic energy is much larger than the mean thermal energy. The acceleration mechanisms are independent of whether the shock is laminar or

turbulent as long as the waves associated with the turbulence do not affect the energetic electrons.

The two acceleration mechanisms are the shock drift and compression mechanisms. The shock drift mechanism occurs because in the rest frame of nonparallel magnetosonic shock waves there is a $\underset{\sim}{V} \times \underset{\sim}{B}$ electric field $\underset{\sim}{E}_y$ due to the motion of the upstream and downstream plasma, where $\underset{\sim}{V}$ is the fluid velocity. For the shock geometry in Figure 4.1., $\underset{\sim}{E}_y = \hat{y}|\underset{\sim}{V}_s||\underset{\sim}{B}_1|\sin\psi_1$, where $\underset{\sim}{V}_s$ is the shock velocity in the upstream plasma rest frame. As pointed out in Armstrong et al. (1977), the $\nabla|\underset{\sim}{B}|$ guiding center drift of electrons interacting with the shock is antiparallel to $\underset{\sim}{E}_y$. Thus, the $\nabla|\underset{\sim}{B}|$ drives a current $\underset{\sim}{J}$ and the electrons comprising the current experience a $\underset{\sim}{J}\cdot\underset{\sim}{E}_y$ energy gain. The compression mechanism works because of the difference in the plasma bulk flow velocity across the shock front (Axford et al., 1977; Bell, 1978). Electrons that diffuse back and forth across the shock in its frame are accelerated by reflection of approaching upstream scattering centers and decelerated by reflection off receding downstream scattering centers. These postulated scattering centers are convected by the bulk plasma motion so that the approaching centers move faster than the receding ones. Thus electrons gain a net energy by being effectively compressed between upstream and downstream scattering centers.

To find the post-shock energies and pitch angles we go to an inertial frame in which both the upstream and downstream $\partial \underset{\sim}{B}/\partial t$ and $\underset{\sim}{V}\times\underset{\sim}{B}$ electric fields are simultaneously zero (EEZ frame) shown in Figure 4.1(b). In this frame, the plasma bulk velocity is along $\underline{B}$ and electrons gain no energy from the shock. For the shock waves that are planar in the x-z plane of Figure 4.1 and for which $\underset{\sim}{V}_s$, ψ_1 and ψ_2 (angle between $\hat{n}$ and $\underset{\sim}{B}_z$) do not vary in space or time, Pesses et al. (1981) have calculated the energy gains and pitch angle changes that result from the shock drift and compression mechanisms analytically given the post-shock pitch angle in the EEZ frame. The pitch angle α is the polar angle between the particle velocity $\underset{\sim}{v}$ and $\underset{\sim}{B}$. The effects of the shock drift mechanism are calculated by transformations between the shock rest frame and the EEZ frame. The effects of the shock compression mechanism are calculated by transformations between the pre- and post-shock plasma rest frame of the electron and it is assumed that the scattering centers are at rest.

The reader is referred to Pesses et al. (1981) for the detailed results. We shall merely note the general properties. Electrons reflected at fast mode shocks gain energy only in the component of their velocity parallel to the magnetic field. The minimum number of times an upstream electron must reflect off the shock front, N, for its speed to exceed $(3)^{1/2}\ v_e$ in the upstream plasma is (Pesses, private communication)

$$N > 1.6\, v_{ni} \sec \psi_1 / v_e \,, \qquad (4.2.1)$$

where v_{ni} is the normal component of the upstream bulk velocity in the shock rest frame. It is possible that counterstreaming electrons become unstable and excite Langmuir waves for a smaller number of reflections. Particles transmitted at fast mode shocks gain energy primarily in the component of their velocity perpendicular to the magnetic field. There are instabilites which can convert such an anisotropic distribution into electron cyclotron waves and these could nonlinearly couple to Langmuir waves. However, the details remain to be worked out. Both the magnitude of $\underset{\sim}{E}_y$ and the velocity of the $\nabla|\underset{\sim}{B}|$ drift increase with increasing values of ψ_1 and thus also the gain in electron energy per encounter.

In summary it appears that our knowledge of collisionless shock waves is now sufficiently complete so that viable mechanisms for producing electron beams and Langmuir waves can be constructed. However, to date the only quantitative calculation is that of Smith (1972b) and this needs to be repeated taking into account the potential drop across the shock. In general the upstream and downstream beam producing potential of a shock increases with ψ_1 and, since this should be reflected in its plasma emission potential, an explanation for the patchy nature of type II emission (cf. Section 2.3) appears possible.

4.3. Radiation Mechanisms

The question of the radiation mechanisms in this case is frought with all the problems for type III bursts (Section 3.5,6) together with the uncertainty in the beam characteristics and density. Conteracting this problem is the relative slowness with which the burst occurs (cf. Fig. 1.1) and the richness of structure (Section 2.3). We know that in the majority of type II bursts the fundamental and harmonic are of comparable magnitude and brightness temperatures reach 10^{11} K. It was shown by Smith (1972b) that without amplification, the fundamental at meter wavelengths would be more than five orders of magnitude less intense than the second harmonic. In any case without amplification, the brightness temperature of the fundamental cannot exceed 3×10^9K (Smith, 1970). Thus amplification of the fundamental is essential.

The problem of amplifying fundamental radiation in a plasma with random density inhomogeneities was analyzed by Smith and Riddle (1975). They showed that inhomogeneities of scale 35 km and strength $\varepsilon = (\delta n^2)^{1/2}/n = 0.016$ at the 80 MHz plasma level would not allow amplification. Thus a model with homogeneous Langmuir waves over scale sizes of 100 km or more as in Smith (1972b) is unlikely to be applicable. Smith and Sime (1979) studied the amplification of Langmuir waves in a plasma with random density inhomogeneities and showed that inhomogeneities of scale size $\sim$50 km at 0.5 A.U. with ε =

4.8×10^{-3} would allow amplification only in certain clumps or spikes where the energy density in Langmuir waves could reach high levels. The value of ϵ in their analysis was determined from interplanetary scintillation data. There is no method of directly measuring density inhomogeneities at the 80 MHz plasma level, but, since these inhomogeneities presumably originate at the sun and are only smoothed out by the solar wind, they are only likely to be stronger at this level. The area downstream from a turbulent shock is likely to be turbulent and have a variety of low frequency waves present as well.

Thus a general picture of emission from type II shocks is the following. The emission mechanism is plasma emission near the fundamental and second harmonic (Smith, 1970, 1972a; Melrose, 1980a). Langmuir waves are produced by beams produced in the shock or accelerated between the shock and scattering centers both upstream and downstream from the shock. Because of the presence of density inhomogeneities and/or low frequency waves the beams relax and produce Langmuir waves only in spatially localized clumps of scale $\sim$35 km at the 80 MHz plasma level. The Langmuir waves in these clumps are at a sufficiently high level to allow the fundamental to be amplified up to the same level as the second harmonic. In the region downstream from the shock some fundamental emission may also be produced by coalescence of Langmuir waves with low-frequency waves (cf. Section 5.4). The Langmuir waves are

likely to have a more or less isotropic distribution if produced by counterstreaming beams or due to induced scattering (Smith, 1970) and/or because of scattering off of the density inhomogeneities. As explained in Smith (1972a) and Section 3.5 this will greatly facilitate production of the second harmonic. The spontaneous scattering considered in Smith (1972a) is unlikely to be important.

Normally the scattering centers and area of beam relaxation occur close to the shock and we see normal type II emission. When the regions upstream and downstream from the shock are well differentiated in density split bands occur (cf. Section 2.3). When the scattering centers are sufficiently far from the shock and the shock is sufficiently oblique, we see herringbone structure due to the much larger beam relaxation regions. If there is enhanced beam relaxation near the shock a "backbone" is present in the herringbone structure. This whole scenario is quite speculative at present and needs to be worked out in detail. However, it appears that our knowledge of the plasma physics involved is now or soon will be sufficiently complete to make such an endeavor worth the effort.

5. RADIO EMISSION FROM MOVING PLASMOIDS AND OTHER TRAPS

We move now to a greyer area of solar radio emission with some overlap with the current sheets of Section 4 since such sheets may be embedded in the configurations of this section. This area is greyer because the emission takes place in regions which are atypically dense and/or have an atypically high magnetic field so that we are sampling a special region of the corona in some sense which often is only seen by its radio emission. Thus independent means of establishing density and/or magnetic field, etc., are often absent and the interpretation of the observations is necessarily more speculative.

5.1. Plasmoid and Other Trapping Configurations

This subsection could be subtitled "detached and rooted coronal loops" including the possibility that detached loops close on themselves and form complete toruses. The quantitative analysis of loops and their evolution is in its infancy since their importance in flare physics was only brought out by the Skylab observations (Sturrock et al., 1980). All of the quantitative analyses assume a form for the magnetic field since it has not been measured directly. Most of the analyses of the density and temperature structure of loops have been carried out on large long lived loops (e.g., Foukal, 1978) which may be related to type I emission, but are most likely unrelated to moving type IV emission. Thus the

basic configurations for the magnetic field can only be inferred from the observations and modeling and, except in a few cases, the same is true for the density and temperature. The only modeling which has been done is by Altschuler, Nakagawa and Lillequist (1968) for photospheric conditions. These results have been used by Dulk and Altschuler (1971) in the "cartoon approximation" for plasmoid type moving type IV bursts as shown in Figure 5.1. Here a toroidal current ring with its own poloidal magnetic field moves outward through a decreasing background poloidal field. While this configuration is able to explain many of the features of plasmoid type moving type IV bursts, it is not clear how it might evolve from an expanding magnetic arch which would favor development of a toroidal magnetic ring.

A toroidal ring could explain the occurrence of double sources in moving type IV bursts which are oppositely circularly polarized. It could also evolve naturally from an expanding magnetic arch which is ejected from the sun simply by reconnection of the feet of the loop which might be squeezed together in the ejection process. Some modeling work on toroidal magnetic rings has been done by Lillequist, Altschuler and Nakagawa (1971) and Altschuler et al. (1973) who included the effect of the Hall term in Ohm's law which is important for densities $n < 10^7$ cm^{-3} and scale lengths less than 2×10^4 cm. However, no work has been done modeling large toroidal rings

for coronal conditions which is the case possibly relevant to moving type IV bursts. A problem with toroidal rings is that moving type II sources sometimes switch from a single source with o-mode polarization to a double source with o-mode and x-mode polarizations during their evolution. They can also break up into as many as four sources, all with the same sense of polarization. A toroidal ring when small would be expected to have little net polarization because polarizations from different regions would tend to cancel for most viewing angles. A poloidal field as in Figure 5.1 where there is a concentration of field in one direction can much more easily explain a single sense of polarization although why this would always be o-mode is a difficulty for gyrosynchrotron emission. A further difficulty is why an observer should be always looking within 30° of the direction of the strong field which is needed to explain strong polarization (Wild and Smerd, 1972). This problem becomes especially severe for sources near the limb of the sun which are often observed to have high degrees of polarization in the late phases of events.

In summary, plasmoid type configurations of a hybrid variety with both toroidal and poloidal components appear to offer the best possibility for explaining the observations, but even then there are difficulties with pure gyrosynchrotron emission. As pointed out by Robinson (1977), a poloidal field is inevitably accompanied by a toroidal field in any case if

the plasmoid is to be force-free and thus stable. Any gradient in the poloidal field produces a toroidal field under the force-free condition. How this mix of poloidal-toroidal field is created remains unclear. Still a plasmoid with its own magnetic field remains a likely candidate for some moving type IV bursts.

The alternate basic configuration is a loop with some attachment, however loose, to the background solar field. The magnetic field is primarily toroidal and runs along the loop. Any current running along the loop will create a poloidal field component. The main problem with this type of configuration is containment of fast electrons. There are two possible ways in which this could occur: 1. The loop is rooted in stronger magnetic fields so that electrons moving to higher fields with finite pitch angles mirror successively. We then have a magnetic trap. 2. Electrons with velocities $v > 43\ v_A$ excite whistler waves (Melrose, 1974) which scatter these electrons and keep them confined to the top or end of the loop. This process is called resonant scattering. Just how long and under what conditions the first alternative will work in the presence of losses is discussed in Section 5.3. The quantitative analysis of the second alternative is just being worked out (Dulk, private communication) since it may have special relevance to the observed propensity of microwave bursts to be confined to the tops of loops (cf. Section 2.1). In terms of

energy the criterion $v > 43\ v_A$ becomes (Melrose and Brown, 1976)

$$E > E_{min} \approx 5.2(v_A/10^8\ \text{cm s}^{-1})^2\ \text{keV} \qquad (5.1.1)$$

and the Alfvén speed

$$v_A = 2.2 \times 10^{11} B n^{-1/2}\ \text{cm s}^{-1} . \qquad (5.1.2)$$

For typical loop densities and magnetic fields v_A lies in the range $1\text{-}4 \times 10^8$ cm s^{-1} and thus $E_{min} \approx 6\text{-}85$ keV. Taking the lower limit, which is probably more applicable to type I and moving type IV emission, it is possible in principle to contain electrons which could radiate by plasma radiation.

There are many facets of the loop configuration which remain to be worked out. For example, what is the effect of a steady current on the resonant scattering process? Does counterstreaming of fast electrons mirroring in a trap lead to instability? About all that can be done now is to take model distribution functions, put them in a loop and see how they evolve in the manner of Melrose and Brown (1976). Still, as a model for microwave, type I, and some moving type IV bursts, a loop with containment is a strong candidate for the basic configuration.

5.2. Sources of Electrons in Plasmoids and Traps

To be able to study emission mechanisms in the configurations of Section 5.1 we need to know the energization and loss processes for electrons which are considered in the

following two sections. As stated in Section 1 the initial energization of electrons will not be considered although some of the mechanisms for the continuing energization of electrons are the same. The main possibilities are direct electric field acceleration as in a current carrying loop with tearing mode instabilities and acceleration by hydromagnetic turbulence generated as the configuration moves through the surrounding medium. There are also currents associated with contained plasmoid configurations, but since the exact configuration remains unknown, it is difficult to analyze this possibility for tearing instabilities in detail. Thus we shall only consider tearing instabilities in a loop in a general way which could be applied to plasmoid configurations. Similarly, although the motion of plasmoids and loops through the surrounding medium is almost certain to generate hydromagnetic turbulence, the exact spectrum of the turbulence has not been worked out for specific motions. Hence we shall only consider acceleration by hydromagnetic turbulence for an arbitrary level of the turbulence.

The theory of particle acceleration and heating due to fast tearing modes has been considered by van Hoven (1979) and Spicer (1980) and is also considered in the article by Spicer in this volume. The basic characteristic of interest is the rate at which electrons in a current carrying loop gain energy. The actual energy gain occurs in very small regions in

a very inhomogeneous manner, but since we are only interested in the emission averaged over the loop resulting from the spatially averaged distribution function, this is of little concern. The pitch angle distribution is of importance and we shall take the result of Spicer (1980) in agreement with the results of Smith (1979) that tearing modes result primarily in heating rather than acceleration. Thus we shall take the initial pitch angle distribution as isotropic. Both van Hoven (1979) and Spicer (1980) only consider a single tearing region. The rate of energy release in the volume of the loop is given by (Spicer, 1977)

$$\frac{dE}{dt} \approx \frac{\gamma B_p^2 \Delta V}{4\pi} \qquad (5.2.1)$$

where γ is the growth rate, B_p is the poloidal field and ΔV is the incremental volume of the loop in which the tearing mode occurs. A rough estimate for the growth rate for fast tearing modes is (Spicer, 1980)

$$\gamma \approx S^{2/3}/\tau_R \,, \qquad (5.2.2)$$

where $S = \tau_R/\tau_A$ is the magnetic Reynolds number and the resistive diffusion time

$$\tau_R = \frac{4\pi(\delta\ell)^2}{\eta c^2} \,. \qquad (5.2.3)$$

Here $\delta\ell$ is the characteristic gradient scale length and η is the resistivity. The Alfvén transit time $\tau_A = \delta\ell/v_A$.

Further analysis requires the specification of the parameters of a loop and the tearing modes occurring in the loop. We simply state some typical rates for coronal parameters, $n = 10^8$ cm^{-3}, $T_e = 1.6 \times 10^6$K, $B_p = 1$ G and $\Delta V = 10^{26}$ cm^3. Typical growth rates are 10^3 s^{-1} so that from Equation (5.2.1) $dE/dt \approx 8 \times 10^{27}$ erg s^{-1} or 8×10^{-7} erg s^{-1} per electron. It would take 0.2 s to heat an electron to 100 keV, but since the total volume involved is of the order of 10^{32} cm^3, only some fraction of the electrons will be heated as the tearing volume moves within this region. Slower tearing rates and acceleration times are also possible.

Acceleration by hydromagnetic turbulence has been considered by Melrose (1974) using the model of Kulsrud and Ferrara (1971) together with scattering by whistler waves. The basic idea is that electrons interact with low frequency, large amplitude hydromagnetic (HM) waves. The HM waves can cause changes in the pitch angle distribution due to conservation of the adiabatic invariant $E_\perp/B$. The perpendicular energy increases with the magnetic field strength during the first half of the wave cycle and would be returned to the field during the second half cycle in the absence of scattering. Scattering of the electrons transfers some of the gained perpendicular energy to the parallel component which is unaffected by magnetic field variations and the intensity of the HM waves decreases with an increase in electron energy.

The transfer of energy is produced by the scattering and its rate is thus largely determined by the scattering rate ν. Clearly this must be larger than the frequency of the turbulence ω. It is argued by Melrose (1974) that wave-particle interactions are the only known process capable of giving the required scattering rate. The resonant waves are generated by the electrons themselves, undergoing induced emission during the compression phase (increasing B) and reabsorption during the rarefaction. Since the distribution function changes due to the scattering, not all of the whistler waves will be reabsorbed during the second half cycle. Thus, there is a gradual build-up of the wave intensity and scattering effectiveness with a corresponding increase in the acceleration rate. They reach a constant level when the energy density in whistlers is so large that the anisotropy driving the whistlers is removed in one wave period or less.

The acceleration rate after the whistlers reach their saturation level is (Melrose, 1974)

$$\nu_A = \frac{\pi}{4}\omega\varepsilon^2 \frac{\beta_A}{\beta} , \qquad (5.2.4)$$

where $\varepsilon = B_t/B_o$ is the relative amplitude of the turbulence with B_t the turbulent field strength at maximum and B_o the background magnetic field. The electron velocity $v = \beta c$ and $\beta_A c = v_A$. The restrictions on (5.2.4) are:

(a) The mean free path is greater than the wavelength of the turbulence

(b) The scattering rate $\nu \gg \nu_A$

(c) The electrons can resonate with the whistlers [Eq. (5.1.1)]

(d) The whistlers have a sufficient time to grow which means that the density of electrons n_1 being accelerated must satisfy

$$\frac{n_1}{n} \gg \frac{\omega}{\Omega_i} \left(\frac{\gamma\beta}{43\beta_o}\right)^2 , \qquad (5.2.5)$$

where Ω_i is the ion gyrofrequency, $\gamma = (1-\beta^2)^{-1/2}$, and $\beta_o = 43\ \beta_A$. Further application requires specification of the turbulence, and acceleration to $\sim$200 keV will occur on a time scale of a few minutes from turbulence with periods in the range 0.1 to 10 s which is indicated by pulsations of meter-wave continuum radiation (McLean et al., 1971).

5.3. Loss-cone and Collisional Electron Losses

We consider how electrons mirroring in a loop or other trap lose energy. The pitch angle α is the angle between the direction of electron motion and the magnetic field. It is convenient to write distributions in terms of the $\cos \alpha = \mu$. A loss cone distribution is flat out to a value of $\pm\mu_o$ and rapidly falls to zero for larger $|\mu|$. Electrons which are scattered into the loss cone by wave-particle or collisional scattering are lost to the system. The resulting anisotropic pitch angle distribution can lead to the growth of Langmuir waves under certain conditions (Stepanov, 1973; Kuipers, 1974). The energy relaxation rate due to collisions is ν_e

and the deflection rate is ν_D which is the rate at which which pitch angle diffusion occurs. For Coulomb collisions, $\nu_E/\nu_D = 0.5$ since fast electrons are scattered at the same rate by both thermal electrons and ions, but only the interactions with thermal electrons cause energy changes (Trubnikov, 1965). The value

$$\nu_D \approx 10^{-8}\ n\ E^{-3/2}\ s^{-1} \qquad (5.3.1)$$

where E is the electron energy in keV (Melrose and Brown, 1976). There are two simple approximations to the precipitation rate ν_p which is the rate at which energy is lost from the trap. The pitch angle at the edge of the loss cone is α_o and the bounce rate in the trap is ν_b. The two approximations which Kennel (1969) called the weak and strong diffusion limits are:

$$\nu_p \approx \begin{cases} \nu_D & \nu_D << \frac{1}{2}\ \alpha_o^2\ \nu_b \\ \frac{1}{2}\ \alpha_o^2\ \nu_b & \nu_D >> \frac{1}{2}\ \alpha_o^2\ \nu_b \end{cases} \qquad (5.3.2)$$

It has been assumed that $\alpha_o^2 << 1$. These two limits represent approximately full loss cones, respectively. For coronal traps the weak diffusion limit will usually apply.

Without a loss cone as in a closed plasmoid, the only losses are collisional losses between fast electrons and the electrons of the background distribution since collisions with ions only lead to deflections to a good approximation. The

loss rate in this case is just $\nu_E = 0.5\ \nu_D$ with ν_D given by Equation (5.3.1).

5.4. Radiation Mechanisms

The main candidates for the radiation mechanism for moving type IV, type I and microwave bursts are plasma radiation and gyrosynchrotron radiation. Since we have already reviewed plasma radiation in relation to type II and type III bursts (cf. Sections 3.5 and 4.3), we shall only consider applying these results to the bursts mentioned except for type I bursts where coalescence of Langmuir and ion-acoustic waves will be treated. The alternate possibility of gyrosynchrotron radiation will then be reviewed.

In general, plasma emission can be broken up into three parts: 1. Wave source. 2. Transformation of Langmuir waves into radiation . 3. Propagation of radiation from the source to the observer. We consider this scenario for each of the burst types of this section. Because of the difficulties noted in Section 3.5,6 with radiation in the strong turbulence regime, we limit the discussion to weak turbulence emission processes which is consistent with all the published results on these bursts. As noted in Section 2.2 we do not intend to treat the theory of microwave bursts in detail. The only microwave emission which requires plasma emission at present is the fine structure in microwave type IV bursts although some microwave bursts recently observed are pushing the gyrosynchrotron theory

to its limits. The theory for the microwave type IV fine structure would be similar either to plasma emission for moving type IV or type I bursts.

We begin with plasma emission from a moving type IV burst for either the expanding arch or plasmoid type source. Because of the rather open nature of the basic configuration (cf. Section 5.1) and the consequent open nature of the electron population (cf. Section 5.2), the source of Langmuir waves is fairly arbitrary. It should be able to sustain the losses due to Langmuir waves and those of Section 5.3 if continuous acceleration is not required. The most likely types of electron distribution for an arch or a plasmoid are a "gap" or plateau as shown in Figure 5.2. A "gap" distribution (Melrose, 1975) is one which peaks at a velocity $v = v_o$ and rapidly falls for $v < v_o$ with a region of velocity space between the thermal distribution and the nonthermal peak in which $n_l \lambda_D^3 < 1$, i.e. the density n_l is less than one particle per cubic Debye length λ_D. When the distribution is unidirectional, we have the beam treated in Sections 3 and 4. The number density of particles with $v \approx v_o$ must be sufficiently high to dominate over the thermal particles in the emission and absorption of Langmuir waves with $v_{ph} \approx v_o$, where v_{ph} is the phase velocity. In the case of an arch the most likely distribution is an anisotropic gap distribution with the anisotropy caused by loss of particles through the

loss cone and the gap created by resonant scattering and/or collisional losses. In a plasmoid there is no loss cone and collisions tend to create a gap, but quasilinear relaxation (Section 3.2) tends to fill in the gap with a plateau resulting in a distribution intermediate between Figures 5.2(a),(b). For times long compared to relaxation and collision times but still short compared to the lifetime of the plasmoid, the distribution should be isotropic.

The plasma emission from an arch depends on the ratio of suprathermal to background plasma densities n_1/n. The growth rate for Langmuir waves due to the loss cone instability was estimated by Melrose (1980a) as

$$\gamma(k,\theta) \approx \pi \frac{n_1}{n} \omega_{p\Phi} G(\theta), \qquad (5.4.1)$$

where $G(\theta)$ is a function depending on the details of the distribution function f. The main point is that this growth rate is large compared to collision times so that the instability should saturate giving an energy density in Langmuir waves comparable with the energy density in the trapped electrons. For example, for $n_1/n \approx 10^{-3}$ and 30 keV electrons, the Langmuir waves will have an effective temperature $T_p \approx 10^{14}$K. Since there will be counterstreaming in the source the Langmuir wave distribution should be approximately isotropic resulting in second harmonic emission with $T_b < T_p$. Although there is some controversy over the

expected polarization characteristics, the degree of polarization should be weak. As in Section 4.3, unless the fundamental is amplified, it will be much weaker than the second harmonic. It could be suppressed by density inhomogeneities or lack of sufficient optical depth. This would be consistent with observations since moving type IV sources generally appear to be well above the plasma level. However, because of scattering the fundamental source can also appear much higher than its true position. Since the bursts only have high brightness temperature with low degrees of polarization (Duncan, 1981), there is no compelling need for fundamental emission.

The plasma emission from a plasmoid with an isotropic gap f is limited to $T_b < 3 \times 10^9$K for nonrelativistic electron energies (Melrose, 1980a) and if the gap is partially filled in even less. Thus, without some continuous acceleration process, a plasmoid with plasma emission is only a possible model for the late phases of many moving type IV bursts. Only fundamental emission could lead to the observed high degrees of circular polarization.

Proceeding to type I bursts and continuum, we note that because of the strong o-mode polarization up to 100% (Section 2.5), plasma radiation could only be near the fundamental. Thus the problem here is how to obtain fundamental $T_b > 10^{10}$K without observable second harmonic

emission. The recent approaches to this problem have invoked the coalescence of Langmuir waves with ion-acoustic waves (Melrose, 1980c; Benz and Wentzel, 1981). The source of Langmuir waves according to Melrose (1980c) is a loss cone instability which is just strong enough to overcome collisional losses of Langmuir waves and maintain the waves in a marginally steady state. The plasma waves then build up over a time of order $\gamma_c^{-1} \approx 0.1\text{-}1$ s, where γ_c is the collisional damping rate. For a 5 keV beam with characterstic velocity $v_o \approx 10^9$ cm s^{-1}, the waves build up over a distance $v_o\gamma_c^{-1} \approx 10^3\text{-}10^4$ km and it is assumed that Langmuir waves occur over such time and distance scales. According to Benz and Wentzel (1981) the source of Langmuir waves may be trapped nonthermal electrons from previous burst sources. The idea is that current instability in an unspecified manner accelerates electrons. They become trapped by an anomolous-cyclotron instability (Papadopoulos and Palmadesso, 1976). The current instability is also the direct source of ion-acoustic waves which thus have an effective temperature $T_s >> T_p$.

The emission process is the coalescence of a Langmuir and an ion-acoustic or other low frequency wave. For simplicity, we confine the discussion to ion-acoustic waves. Benz and Wentzel have argued that these are the most likely candidate because they saturate at a relatively high level. This in turn allows an optical depth of order unity to be

reached for a source thickness of 0.1 km. Melrose argues for a minimum source size of 10^3 km, but he does not consider in detail the excitation condition for the ion-acoustic waves. Benz and Wentzel do consider the excitation condition and conclude that the ion-acoustic waves must be confined to a thin sheet. In Melrose the emission is controlled by the Langmuir waves. In Benz and Wentzel T_b is controlled by the Langmuir waves, but the optical depth is controlled by the ion-acoustic waves. This allows them to obtain $T_b \leq 4 \times 10^{13}$K without a detectable harmonic ($<10^{-20}$ erg cm^{-2} s^{-1} Hz^{-1}). Because Melrose has a source size of 10^3 km, he expects a detectable harmonic (10^8K) for a bright type I burst with $T_b = 10^{10}$K. Of course Benz and Wentzel will not have a detectable harmonic only to the extent that the Langmuir waves are confined to thin sheets as for the ion-acoustic waves and they have not given any mechanism for such confinement. The continuum according to Melrose is due to coalescence of stable Langmuir and low-frequency waves in a large source. Benz and Wentzel are more specific. They suggest that low-frequency waves with small k decay into low-frequency waves with sufficiently high k to combine with Langmuir waves to produce radiation. Since the k of the radiation is small, small k low-frequency waves are of no use without some further process. Benz and Wentzel suggest that whistlers and lower-hybrid waves are likely candidates for the low frequency waves.

Moving to gyrosynchrotron radiation, we begin again with moving type IV bursts. As noted in Section 2.4, until recently this was the accepted emission mechanism for these bursts and is still possibly the best explanation for the late phases of these events. Gyrosynchrotron emission requires electrons of 100 keV similar to microwave bursts. Dulk (1973) developed the theory of this emission for moving type IV sources and argued that the relatively sharp cutoff at low frequencies is due to synchrotron self-absorption; in other words, when the source becomes optically thick, as it does at low frequencies, only a fraction of the radiation escapes. Robinson (1974) extended Dulk's calculations to the case of inhomogeneous magnetic field configurations. The results are that $T_b \leq 10^9$K and the radiation is polarized in the x-mode up to 100%, for an optically thin source, but depends sensitively on the viewing angle. The primary success of the gyrosynchrotron hypothesis is an explanation for why the degree of emission increases as the source moves out which is applicable mainly to plasmoid type sources. With self-absorption both the ordinary and extraordinary mode are comparable and there is little polarization. As the source moves out, it become less self-absorbed and the x-mode becomes dominant leading to high degrees of polarization. There is no analogous explanation with plasma emission. Counteracting this success of gyrosynchrotron emission is the sensitivity of this result to the viewing angle of the observer.

A combined model in which plasma emission dominates for sources close to the sun and gyrosynchrotron emission dominates for sources further out would seem the best choice at present, but clearly more work needs to be done on plasma emission in this context.

Moving to type I emission, gyroemission at low harmonic numbers excited by a beam with large perpendicular velocity has been considered by Mangeney and Veltri (1976). They showed that coupling of unstable whistler and x-mode waves with low frequency MHD waves would stabilize these modes, but that the o-mode would remain unstable. This leads to o-mode radiation of relative bandwidth $3\text{-}4 \times 10^{-2}$ and high directivity. The average opening angle of the radiation is at most 12°. This is the principle success of this model. There is no explanation of the high directivity of type I emission with plasma radiation. Counteracting this success is an explanation of how the beams are accelerated. Mangeney and Veltri's model applies to bursts, but offers no explanation for the continuum.

At the present time it is difficult to judge whether plasma or gyroemission is a better model for type I bursts. Excitation of Langmuir waves by a loss cone instability seems plausible and less ad hoc than the beams of Mangeney and Veltri (1976) and a tie-in with the escape of electrons from traps as a source fo storm type III bursts also seems natural. The high directivity of gyroemission, on the other hand, is also

attractive. It is difficult to see how such directivity which is required by the observations (Section 2.5) could come from plasma emission except through a propagation effect. This is an area of research which is bound to be active in the next few years.

6. CONCLUSIONS AND RECOMMENDATIONS

Solar radio astronomy is now at a stage where observations, particularly from satellites, are beginning to provide enough pertinent data to enable theory to be put to the test. This has been true especially for the theory of type III bursts, the most exhaustively studied and supposedly well-understood of all solar emissions. The results are surprising and provocative. Even the very cornerstones of the theory of type III bursts have been challenged. A vigorous period of re-examination of fundamental processes seems to be in order. This should represent a healthy stage in the development of the underlying physics, in which reasonable hypothesis is bridled by reality, and the dominant factors governing emission are finally identified from among speculative alternatives.

We separately present our conclusions and recommendations for the various kinds of radio emissions, beginning with the type III burst.

6.1. Type III Emissions

Above 10 MHz, it is known that the source heights observed by radioheliograph cannot be the true heights of fundamental and second harmonic emission. Scattering and ducting of the emissions off density irregularities have been invoked to construct a reasonable picture, but this is somewhat ad hoc, and even with these processes, the frequencies do not relate properly to the quiescent local plasma frequencies, and

density enhancement seems to be required. The observed polarizations at these frequencies also have not been explained by theory (Melrose, 1980b, 1972).

Emissions below 1 MHz are usually identified as second harmonic, although this appears to create irreconcilable difficulties for the causative role of either Langmuir waves or the (high flux) 5-30 keV electron streams which drive them. Some of these difficulties disappear if the emissions can be re-identified as fundamental, but then, once more, it is necessary to postulate strong scattering off density irregularities. The possibility that the observed source positions are not the true source positions ought to be explored seriously for emissions below 1 MHz.

Clearly, what is needed is a positive identification of the emissions below 1 MHz as fundamental or second harmonic, and a careful, comprehensive study of density irregularities in the solar wind. It would be especially helpful if the region between 1 and 40 MHz could be probed to determine which member of the high-frequency fundamental-harmonic pair disappears toward lower frequencies. This might be expedited through the use of radio telescopes near the geomagnetic poles (e.g., Alaska and Tasmania), where the peak ionospheric density cutoff can be low, or by satellite-based high frequency dynamic radiospectrographs. Density irregularities could be studied more systematically by scintillation techniques, or, in the

lower corona, by VHF scattering techniques. Microwave scattering from the lower corona has already been attempted as a means of remotely probing Langmuir waves (Benze and Fitze, 1980a,b), and may be further exploited.

It is likely that part of the difficulty in connecting theory with observation lies in an oversimplified picture of the ambient solar wind. We are now beginning to appreciate that the wind has permanent features like a nonthermal ($\sim$10 keV) component of the electron velocity distribution, and low frequency turbulence which may correspond to ion-acoustic waves (and may even be the source of density irregularities). Such features can have important implications for the underlying plasma physics during radio emission events, and can allow the occurrence of stronger incoherent and coherent emission, or even coherent beam emission in the absence of Langmuir waves. These phenomena ought now to be studied theoretically with more confidence and input from observation.

The most recent spacecraft experiments seem to confirm that the electron streams associated with type III bursts do drive Langmuir waves unstable, even if their relation to the radio emissions remains in question because of their low intensity, occasional absence, and consistently delayed arrival. The theory of the nonlinear saturation of Langmuir waves is complicated by the fact that a number of unrelated nonlinear mechanisms such as plateau formation, induced

scatter, and self-focusing, come into play simultaneously at wave energy densities about 10^{-5} times the background electron energy density. The interplay of all these effects against the background of a realistic corona and solar wind will be one of the tasks of theory in the coming years. Until the properties of Langmuir turbulence, which underlies all plasma emission processes, are well understood, there can be no complete and self-consistent calculations of emissivities and polarizations of the related bursts.

6.2. Type II Bursts

Here, it is desirable to have spacecraft observations of the electron distributions, plasma waves, and radiation of the same variety and quality as for type III bursts, and, in addition, to gather direct data concerning the related shocks. Theoretically, shock heating and beam selection mechanisms should be reconsidered for interplanetary shock parameters, and beam acceleration and relaxation properties should be studied further. The effect of large- and small-scale density inhomogeneities should be taken into account for both plasma waves and amplified fundamental emission. Execution of this program would result in the same confrontation of theory and observations for type II bursts as outlined in Section 6.1 for type III bursts.

6.3. Moving type IV bursts

On the observational side, more multi-frequency interferometer measurements are necessary, and possible correlations with coronal transients need to be examined in more depth. Theoretically, the MHD stability of moving arches and plasmoids should be established, and continuous acceleration processes studied. Controversy over the polarization characteristics of plasma emission in a magnetic field should be resolved (for the type III burst problem as well).

6.4. Type I Bursts

Very high time resolution (better than 10 ms) observations might enable a determination to be made as to whether or not there is any short time-scale structure within bursts. Multi-frequency interferometer observations might help determine the relationship of type I storms to storm type III bursts more precisely. Theoretically, MHD studies of localized current channels in solar arches would be informative. Wave production and electron acceleration in the arches should also be treated.

6.5. General Recommendations

As we have already stressed in connection with type III bursts, it is necessary to bridge the gap in frequencies between ground-based (>5 MHz) and space (<1 MHz) observations of emissions. In addition to the suggestions made in 6.1, we

recommend continuing and augmented support for the Clark Lake facility.

In a more general vein, continued and improved simultaneous measurements by spacecraft of wave and particle distributions are desirable (such as Lin et al., 1981). As for ground observations, it may be possible to better adapt the VLA for solar applications. Specifically, the capability for measuring circular polarization should be improved to an accuracy <1%; the dynamic range should be extended and adequate calibration for solar observations should be provided.

In the area of theory, continued and increased support is essential in order to complement the prolific and productive observational program, and to meet the challenges this program continues to provide to plasma theorists.

ACKNOWLEDGMENTS

One of us (M.V.G.) gratefully acknowledges the help and encouragement of the CSIRO Solar Radiophysics group, and the Department of Theoretical Physics at the University of Sydney during the writing of this review. We are also indebted to G. Dulk, R. Lin, K. Sheridan, R. Grognard, D. Melrose, M. Kundu, M. Pesses and R. Stewart for helpful conversations. This work was supported by National Aeronautics and Space Administration Grant No. NAGW-91, National Science Foundation Grants No. ATM-7916837 and ATM-8020426, and Air Force Office of Scientific Research Grant No. 80-0022.

REFERENCES

Altschuler, M. D., Nakagawa, Y., and Lilliequist, C. G.: 1968, Solar Phys. 3, 466.

Altschuler, M. D., Smith, D. F., Swarztrauber, P. N., and Priest, E. R.: 1973, Solar Phys. 32, 153.

Alvarez, H., and Haddock, F. T.: 1973, Solar Phys. 29, 197.

Alvarez, H., Haddock, F. T., and Lin, R. P.: 1972, Solar Phys. 26, 468.

Alvarez, H., Haddock, F. T., and Potter, W. H.: 1974, Solar Phys. 34, 413.

Armstrong, T., Chen, G., Sarris, E., and Krimigis, S.: 1977, Study of Travelling Interplanetary Phenomena, M. Shea, D. Smart, and S. Wu (eds), Dordrecht, Reidel, p. 367.

Axford, W., Leer, E., and Skadron, G.: 1977, Proc. 15th Int'l Cosmic Ray Conf., Vol. II, p. 132.

Bardwell, S., and Goldman, M. V.: 1976, Astrophys. J. 209, 912.

Bell, A.: 1978, Mon. Nat. Roy. Astron. Soc. 182, 147.

Benz, A. O., and Fitze, H. R.: 1980a, IAU Symposium No. 86, Radio Physics of the Sun, M. R. Kundu and T. E. Gergely (eds), Dordrecht, Reidel, pp 247-250.

Benz, A. O., and Fitze, H. R.: 1980b, Astrophys. J., submitted.

Benz, A. O., and Wentzel, D. G.: 1981, Astron. Astrophys., in press.

Boishot, A., and Clavelier, B.: 1967, Astrophys. Lett. 1, 7.

Boishot, A., Riddle, A. C., Pearce, J. B., and Warwick, J. W.: 1980, Solar Phys. 65, 397.

Bougeret, J. L., and Steinberg, J. L.: 1977, Astron. Astrophys. 61, 777.

Bougeret, J. L., and Steinberg, J. L.: 1980, Radio Physics of the Sun, M. R. Kundu and T. E. Gergely (eds.), Dordrecht, Reidel, p. 401.

Bougeret, J. L., Caroubalos, C., Mercier, C., and Pick, M.: 1970, Astron. Astrophys. 6, 406.

Coles, W. A., and Harmon, J. K.: 1978, JGR 83, 1413.

DuBois, D. F., and Rose, H. A.: 1981, Phys. Rev., submitted.

Dulk, G. A.: 1973, Solar Phys. 32, 491.

Dulk, G. A., and Altschuler, M. D.: 1971, Solar Phys. 20, 438.

Dulk, G. A. and Suzuki, S.: 1980a, Astron. Astrophys. 88, 203.

Dulk, G. A., Melrose, D. B., and Smerd, S. F.: 1978, Proc. Astron. Soc. Australia 3, 243.

Dulk, G. A., Melrose, D. B., and Suzuki, S.: 1979, Proc. Astron. Soc. Aust. 3, 375.

Dulk, G. A., Suzuki, S., and Gary, D. E.: 1980b, Astron. Astrophys. 88, 218.

Duncan, R. A.: 1979, Solar Phys. 63, 389-398.

Duncan, R. A.: 1981, Solar Phys., submitted.

Duncan, R. A., Stewart, R. T., and Nelson, G. J.: 1981, IAU Symp. 91 Solar and Interplanetary Dynamics, D. Dryer and D. Rust (eds), Dordrecht, Reidel, in press.

Elgaroy, O.: 1977, Solar Noise Storms, Oxford, Pergamon Press.

Evans, L. G., Fainberg, J., and Stone, R. G.: 1971, Solar Phys. 21, 198.

Evans, L. G., Fainberg, J., and Stone, R. G.: 1973, Solar Phys. 31, 501.

Fainberg, J., and Stone, R. G.: 1971, Astrophys. J. 164, 123.

Fainberg, J., and Stone, R. G.: 1974, Space Sci. Rev. 16, 145.

Fainberg, J., Evans, L. G., and Stone, R. G.: 1972, Science 178, 743.

Fitzenreiter, R. J., Evans, L. G., and Lin, R. P.: 1976, Solar Phys. 46, 437.

Foukal, P.: 1978, Astrophys. J. 223, 1046.

Frank, L. A., and Gurnett, D. A.: 1972, Solar Phys. 27, 446.

Freund, H.P. and Papadopoulos, K.: 1980, Phys. Fluids 23, 139.

C-2

Gurnett, D. A., and Anderson, R. R.: 1977, J. Geophys. Res. 82, 632.

Gurnett, D. A., and Frank, L. A.: 1975, Solar Phys. 45, 477.

Gurnett, D. A., Anderson, R. R., and Jokar, R. L.: 1980, IAU Symposium No. 86, Radio Physics of the Sun, M. R. Kundu and T. E. Gergely (eds), pp. 369.

Gurnett, D. A., Anderson, R. R., Scarf, F. L., and Kurth, W. S.: 1978, J. Geophys. Res. 83, 4147.

Gurnett, D. A., Baumback, M. M., and Rosenbauer, H.: 1978, J. Geophys. Res. 83, 616.

Haddock, F. T., and Alvarez, H.: 1973, Solar Phys. 29, 183.

Haddock, F. T., and Graedel, T. E.: 1970, Astrophys. J. 160, 293.

Hanasz, J., Schreiber, R., and Aksenov, V. I.: 1980, Astron. Astrophys 91, 311.

Hoyng, P., Duijveman, A., Machado, M. E., Rust, D. M. Svestka, A., Boelee, A., de Jager, C., Frost, K. J., Lafleur, H., Simnett, G. M., van Beek, H. F., and Woodgate, B. E.: 1981, Astrophys. J., submitted.

Kellogg, P. J.: 1980, Astrophys. J. 236, 696.

Kennel, C. F.: 1969, Rev. Geophys. 7, 379.

Krall, N. A., and Smith, D. F.: 1975, Astrophys. J. 199, 500.
Gosling, J. T., Hildner, E., MacQueen R. M. Munro, R. H. Poland, A. I., and Ross, C. L.: 1976, Solar Phys. 48, 389.

Kuipers, J.: 1974, Solar Phys. 36, 157.

Kulsrud, R. M., and Ferrara, A.: 1971, Astrophys. Space Sci. 12, 302.

Kundu, M. R.: 1965, Solar Radio Astronomy, New York, Wiley Interscience.

Lilliequist, C. G., Altschuler, M. D., and Nakagawa, Y.: 1971, Solar Phys. 20, 348.

Lin, A. T., Kaw, P. K., and Dawson, J. M.: 1973, Phys. Rev. A. 8, 2618.

Lin, R. P.: 1970, Solar Phys. 12, 266.

Lin, R. P.: 1974, Space Sci. Rev. 16, 189.

Lin, R. P., Evans, L. G., and Fainberg, J.: 1973, Astrophys. Lett. 14, 191.

Lin, R. P., Potter, D. W., Gurnett, D. A., and Scarf, F. L.: 1981, Astrophys. J., submitted.

Lin, R. P., Schwartz, R., Pelling, M., and Hurford, G.: 1980, Bull. Amer. Astron. Soc. 12, 892.

Magelsson, G. R., and Smith, D. F.: 1977, Solar Phys. 55, 211.

Malitson, H. H., Fainberg, J., and Stone, R. G.: 1973, Astrophys. J. 183, L35.

Mangeney, A., and Veltri, P.: 1976, Astron. Astrophys. 47, 165 and 181.

Marsh, K. A., and Hurford, G. J.: 1980, Astrophys. J. 240, L111.

McLean, D. J.: 1971, Austr. J. Phys. 24, 201.

McLean, D. J., Sheridan, K. V., Stewart, R. T., and Wild, J. P.: 1971, Nature 234, 140.

Melrose, D. B.: 1974, Proc. Astron. Soc. Australia 2, 261.

Melrose, D. B.: 1974, Solar Phys, 37, 353.

Melrose, D. B.: 1975, Solar Phys. 43, 211.

Melrose, D. B.: 1977, Izv. Vyssh. Uchebn. Zaved., Radiofiz. 20, 1369. 1977, Radiophys. and Quantum Electron., 20, 945.

Melrose, D. B.: 1980a, Plasma Astrophysics, Vols. 1 and 2, New York, Gordon and Breach.

Melrose, D. B.: 1980b, Space Science Reviews 26, 3.

Melrose, D. B.: 1980c, Solar Phys. 67, 357.

Melrose, D. B.: 1981, Austral. J. Phys., in press.

Melrose, D. B., and Brown, J. C.: 1976, Mon. Not. Royal Astron. Soc. 176, 15.

Melrose, D. B., and Sy, W. N.: 1972, Australian J. Phys. 25, 387.

Melrose, D. B., Dulk, G. A., and Smerd, S. F.: 1978, Astron. Astrophys. 66, 315.

Nambu, M.: 1981, Physical Review, submitted.

Nicholson, D. R., and Goldman, M. V.: 1978, Phys. Fluids 21, 1766.

Nicholson, D. R., Goldman, M. V., Hoyng, P., and Weatherall, J. C.: 1978, Astrophys. J. 223, 605.

Papadopoulos, D., and Freund, H. P.: 1978, Geophysical Res. Lett. 5, 881.

Papadopoulos, D., Goldstein, M. L., and Smith, R. A.: 1974, Astrophys. J. 190, 175.

Papadopoulos, K. and Palmadesso, P. J.: 1976, Phys. Fluids 19, 605.

Parker, E. N.: 1958, Astrophys. J. 128, 664.

Perkins, F. W., Oberman, C., and Valeo, E. J.: 1974, JGR. 79, 1478.

Pesses, M. E., Decker, R. B., and Armstrong, T. P.: 1981, Space Sci. Rev., in press.

Ramaty, R.: 1969, Astrophys. J. 158, 753.

Riddle, A. C.: 1972, Proc. Astron. Soc. Aust. 2, 148.

Riddle, A. C.: 1974, Solar Phys. 35, 153.

Robinson, R. D.: 1974, Proc. Astron. Soc. Australia 2, 258.

Robinson, R. D.: 1977, Ph. D. Thesis, University of Colorado.

Roberts, J. A.: 1959, Aust. J. Phys. 12, 317.

Robinson, R. D.: 1974, Proc. Astron. Soc. Australia 2, 258.

Robinson, R. D.: 1977, Ph. D. Thesis, University of Colorado

Rosenberg, H.: 1976, Phil. Trans. Royal Soc. A 281, 461.

Rowland, H. L., Lyon, J. G., and Papadopoulos, K.: 1981, Phys. Rev. Lett. 46, 346.

Ryutov, D. D., and Sagdeev, R. Z.: 1970, Sov. Phys., JETP 31, 396.

Saito, K.: 1970, Ann. Tokyo Astron. Obs. 12, 53.

Schmahl, E., and Hildner, E.: 1977, Solar Phys. 55, 473.

Sheridan, K. V.: 1967, Proc. Astron. Soc. Aust. 1, 58.

Slottje, C.: 1980, Radio Physics of the Sun, M. R. Kundu and T. E. Gergely (eds.), Dordrecht, Reidel, p. 195.

Slysh, V. I.: 1967, Kosm. Issled. 5, 897; Cosmic Res. 5, 759.

Smerd, S. F.: 1970, Proc. Astron. Soc. Australia 1, 305.

Smerd, S. F.: 1976, Solar Phys. 46, 493.

Smerd, S. F.: 1976, Physics of Solar Planetary Environments, D. J. Williams (ed.), Washington, A. G. U., Vol. 1, p. 193.

Smerd, S. F., and Dulk, G. A.: 1971, Solar Magnetic Fields, R. Howard (ed.), Dordrecht, Reidel, p. 616.

Smerd, S. F., Sheridan, K. V., and Stewart, R. T.: 1975, Astrophys. Lett. 16, 23.

Smerd, S. F., Wilk, J. P., and Sheridan, K. V.: 1962, Aust. J. Phys. 15, 180.

Smith, D. F.: 1970, Adv. Astron. Astrophys. 7, 147.

Smith, D. F.: 1971, Astrophys. J. 170, 559.

Smith, D. F.: 1972a, Astrophys. J. 174, 121.

Smith, D. F.: 1972b, Astrophys. J. 174, 643.

Smith, D. F.: 1972c, Astron. Astrophys. 18, 403.

Smith, D. F.: 1977, Astro. Phys. J. 216, L53.

Smith, D. F., and Fung, P. C. W.: 1971, J. Plasma Phys. 5, 1.

Smith, D. F., and Krall, N. A.: 1974, Astrophys. J. 194, L163.

Smith, D. F., and Riddle, A. C.: 1975, Solar Phys. 44, 471.

Smith, D. F., and Sime, D.: 1979, Astrophys. J. 233, 998.

Smith, D. F., and Spicer, D. S.: 1979, Solar Phys. 62, 359.

Smith, R. A., Goldstein, M. L., and Papadopoulos, K.: 1979, Astrophys. J. 234, 348.

Spicer, D. S.: 1977, Solar Phys, 53, 305.

Spicer, D. S.: 1981, Solar Phys., in press.

Steinberg, J. L. Caroubalos, C., and Bougeret, J. L.: 1974, Astron. Ap. 37, 109.

Stepanov, A. V.: 1973, Soviet Astron.-AJ 17, 781.

Stewart, R. T.: 1974, Solar Phys. 39, 451.

Stewart, R. T.: 1975, Solar Phys. 40, 417.

Stewart, R. T.: 1976, Solar Phys. 50, 437.

Stewart, R. T., and Vorpahl, J.: 1977, Solar Phys. 55. 111.

Stewart, R. T., Howard, R. A., Hansen, S. F., Gergely, T., and Kundu, M.: 1974b, Solar Phys. 36, 219.

Stewart, R. T., McCabe, M. K., Koomen, M. J., Hansen, R. T., and Dulk, G. A.: 1974a Solar Phys. 36, 203.

Sturrock. P. A. et al.: 1980, Solar Flares, Boulder, Colorado Associated University Press.

Suzuki, S., and Sheridan, K. V.: 1977, Radiofizica 20, 1432.

Takakura, T., and Shibahashi, H.: 1976, Solar Phys. 46, 323.

Tidman, D. A., and Krall, N. A.: 1971, Shock Waves in Collisionless Plasmas, Interscience, New York.

Tokar, R. L., and Gurnett, D.: 1980, J. Geophys. Res. 85, 2353.

Trubnikov, B.A.: 1965, Rev. of Plasma Physics 1, New York, Consultants Bureau, p. 205.

Trulsen, T., and Fejer, J. A.: 1970, J. Plasma Phys. 4, 825.

van Hoven, G.: 1979, Astrophys. J. 232, 572.

Weatherall, J. C., Goldman, M. V., and Nicholson, D. R.: 1981, Astrophys. J. 246, in press.

Wild, J. P.: 1950a, Aust. J. Sci. Res. A3, 542.

Wild, J. P.: 1950b, Aust. J. Sci. Res. A3, 399.

Wild, J. P.: 1974, Records of Aust. Acad. Sci. 3, 93.

Wild, J. P., and McCready, L. L.: 1950, Aust. J. Sci. Res. A3, 387.

Wild, J. P., and Smerd, S. F.: 1972, Ann. Rev. Astron. Ap. 10, 159.

Wild, J. P., Murray, J. D., and Rowe, W. C.: 1954, Aust. J. Phys. 7, 439.

Wild, J. P., Smerd, S. F., and Wiess, A. A.: 1963, Annu. Rev. Astron. Astrophys. 1, 291.

Zaitsev, V. V.: 1977, Radiophys. Quantum Electron. 20, 952.

Zaitsev, V. V., and Ledenev, V. G.: 1976, Sov. Astron. Lett. 2, 443 (Russian original page number).

Zaitsev, V. V., Mityakov, N. A., and Rapoport, V. O.: 1972 Solar Phys. 24, 444.

Zakharov, V. E.: 1972, Zh. Eksp. Teor. Fiz. 62, 1745; Sov. Phys. - JETP 35, 908.

Zheleznyakov, V. V.: 1970, Radio Emission of the Sun and Planets, Oxford, Pergamon Press.

Zheleznyakov, V. V., and Zaitsev, V. V.: 1970a, Sov. Astron. - A. J. 14, 47.

Zheleznyakov, V. V., and Zaitsev, V. V.: 1970b, Sov. Astron. - A. J. 14, 250.

FIGURE CAPTIONS

Fig. 1.1 A schematic representation of the radio spectrum during and after a large flare. The low-frequency type III and type I storms preceding and following the flare are not necessarily ingredients. Only one type III burst has been drawn although a group of approximately ten occurs at the flash phase. Only the envelopes of the respective type IV bursts have been drawn and usually only parts of them are filled. The height scale on the right-hand side corresponds to the plasma level of the frequency scale on the left-hand side (after Rosenberg, 1976).

Fig. 2.1 Early examples of harmonically related pairs of type III bursts recorded with a 40-240 MHz spectrograph at Dapto, Australia in 1953. In the right-hand column the seven bursts are replotted with the harmonic band shifted 2:1 in frequency. The displacement, mostly leftward, of the harmonic bands indicates harmonic ratios <2 (Wild et al., 1954).

Fig. 2.2 Dynamic spectrum and half-peak brightness contours from the Culgoora radioheliograph, for a fundamental-harmonic type III burst at the limb. The heavy solid line is interpreted as emission at $2f_p$ (harmonic

emission at 160 MHz. The medium solid line is $2f_p$ emission at 80 MHz, and the medium dashed line is f_p (fundamental) emission at 80 MHz. The light lines show the $2f_p$ (solid) and the f_p (dashed) emission at 43 MHz. (Stewart, 1976).

Fig. 2.3 A type III burst observed between 1 MHz and 30 kHz by the IMP-6 satellite experiment. The insert figure illustrates the observed spin-modulation at a frequency of 250 kHz, while, for the main figure, only the burst envelopes are shown for clarity (Fainberg et al., 1972).

Fig. 2.4 The volume emissivity as a function of radial distance from the Sun, determined from 36 type III radio bursts detected by IMP-8 and ISEE-1. Frequency components common to one event are linked by straight lines. (From Gurnett et al., 1980)

Fig. 2.5 Events showing a power law dependence of radio flux on high energy electron flux (>18 keV). The slopes of the fitted straight lines (equal to the power law index, α) fall into two distinct groups. Events a-d have $\alpha \sim 1$; events e-g have $\alpha = 2.4$; events h and i show an abrupt transition from $\alpha \sim 1$ to $\alpha \sim 2.4$ (Fitzenreiter et al., 1976).

Fig. 2.6 Electric field intensities and electron fluxes versus time for an event studied from the ISEE-3 satellite. (a) Top panel shows intensity, measured in four broad frequency bands. Black areas show 64 s averages, solid lines give peak intensity, measured every 0.5 s. Smoothly varying profiles in 100 and 56.2 kHz channels show two type III bursts, but only the second is of interest here. Impulsive emission in the 31.1 and 17.8 kHz channels are electron plasma (Langmuir) waves. (b) Omnidirectional electron fluxes from 2 keV to >200 keV, showing velocity dispersion. No significant change in flux is observed below ∿2.5 keV.

Fig. 2.7 Synthesis of data to construct a 1-D velocity distribution function of the electrons as a function of time. Each succeeding distribution within a panel is shifted to the right in velocity by 2×10^9 cm/sec. The distribution averaged over 20 minutes prior to the event onset is indicated by the solid dots in panel (a). 64 s measurements of the distribution during the event are shown every 5 min thereafter. (Lin et al., 1981)

Fig. 2.8 A plot of the peak electric field strength for all of the plasma oscillation events associated with type III bursts (detected to date) as a function of radial distance from the sun.

Fig. 3.1 Inhomogeneous 1-D quasilinear calculation of simultaneous stream and Langmuir spectral evolution. The electron stream distribution function, and the corresponding Langmuir wave distribution are shown at five different times at a single spatial point, 2×10^9 meters above the Sun. The Langmuir distribution is plotted as a function of the phase velocity, ω_p/k. Both velocity dispersion and reabsorption are evident. (Magelssen and Smith, 1977).

Fig. 3.2 Solutions to the stream-driven Zakharov eqn. in two dimensions, relevant to a type III burst at 0.5 AU. Contours of equal $|E_{\underline{k}}|$ are plotted in k-space. The beam-driven modes lie in the rectangle, and are randomly-phased with respect to one-another. The central wave number is $k_o/k_D = 0.011$. (a) Time t_1, (b) Time, t_2, showing induced formed scatter off ions to lower wave member, and off axis modulational instability. (c) Is at time t_3, after collapse is underway. (From Hafizi et al., 1981)

Fig. 4.1 (a) Shock rest frame with the coordinate system used indicated. The E_y in back of the shock has the same value as E_y in front of the shock. E = 0 frame.

Fig. 5.1 Schematic diagram of a possible plasmoid configuration at one stage of its motion along the diverging coronal magnetic field (after Dulk and Altschuler, 1971).

Fig. 5.2 (a) A gap electron distribution. (b) A plateau electron distribution.

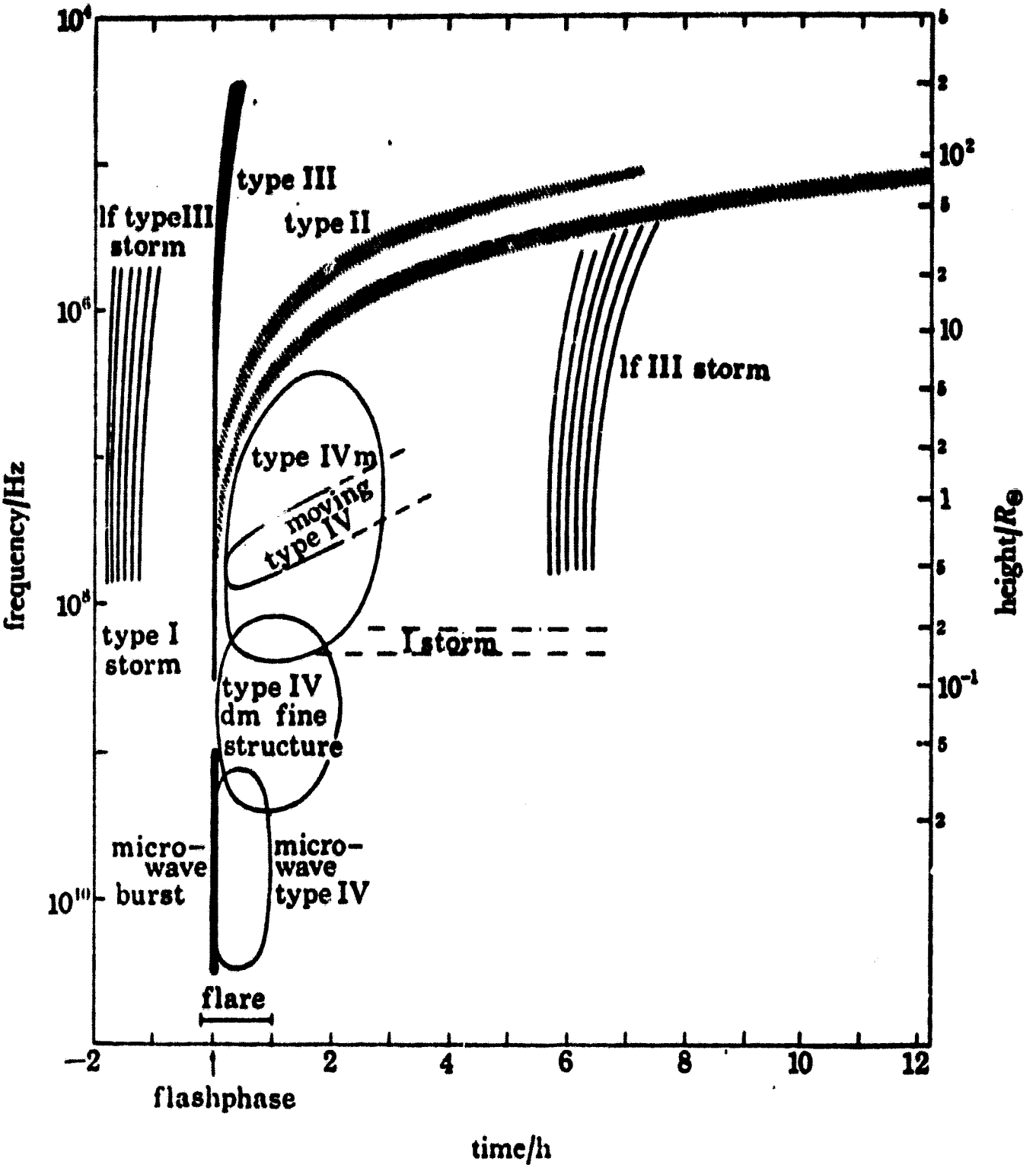
type III
lf typeIII storm
type II
lf III storm
type IVm
moving type IV
type I storm
I storm
type IV dm fine structure
micro-wave burst
micro-wave type IV
flare
flashphase
frequency/Hz
height/$R_\odot$
time/h

Figure 1.1

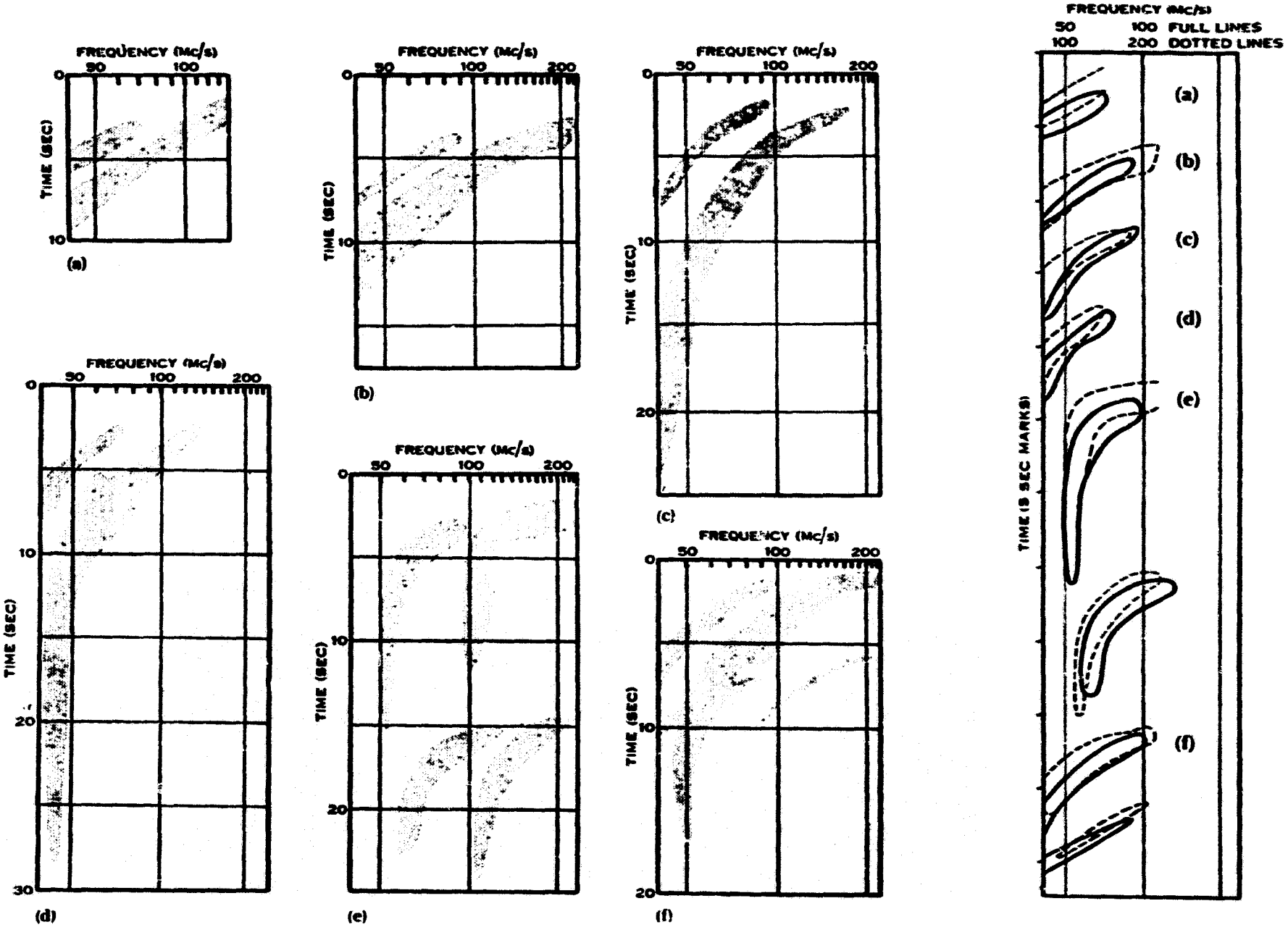
FREQUENCY (Mc/s)
50
100
200
TIME (SEC)
0
10
20
30
(a)
(b)
(c)
(d)
(e)
(f)
FREQUENCY (Mc/s)
50 100 FULL LINES
100 200 DOTTED LINES
TIME (5 SEC MARKS)

Figure 2.1

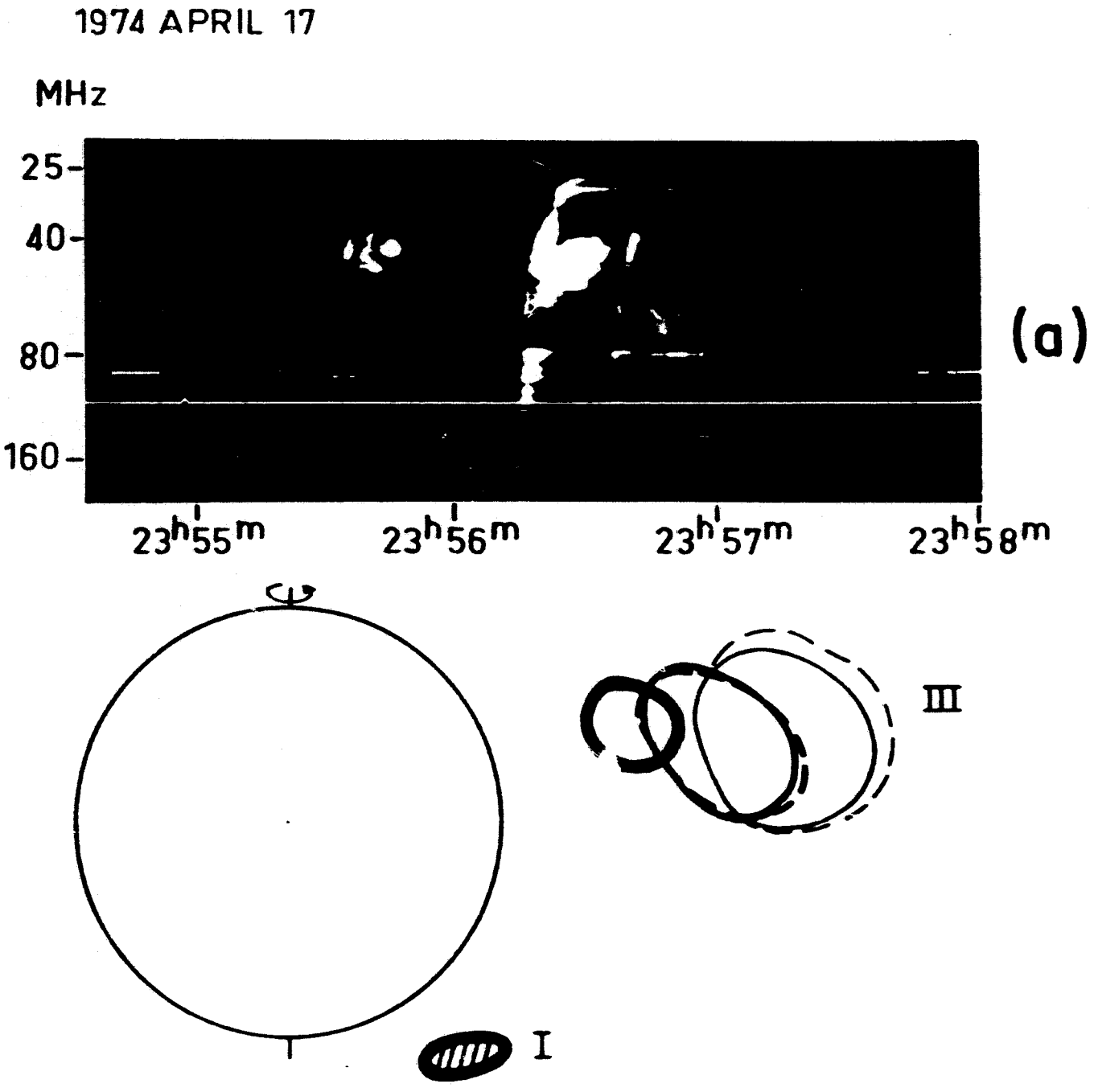

Figure 2.2

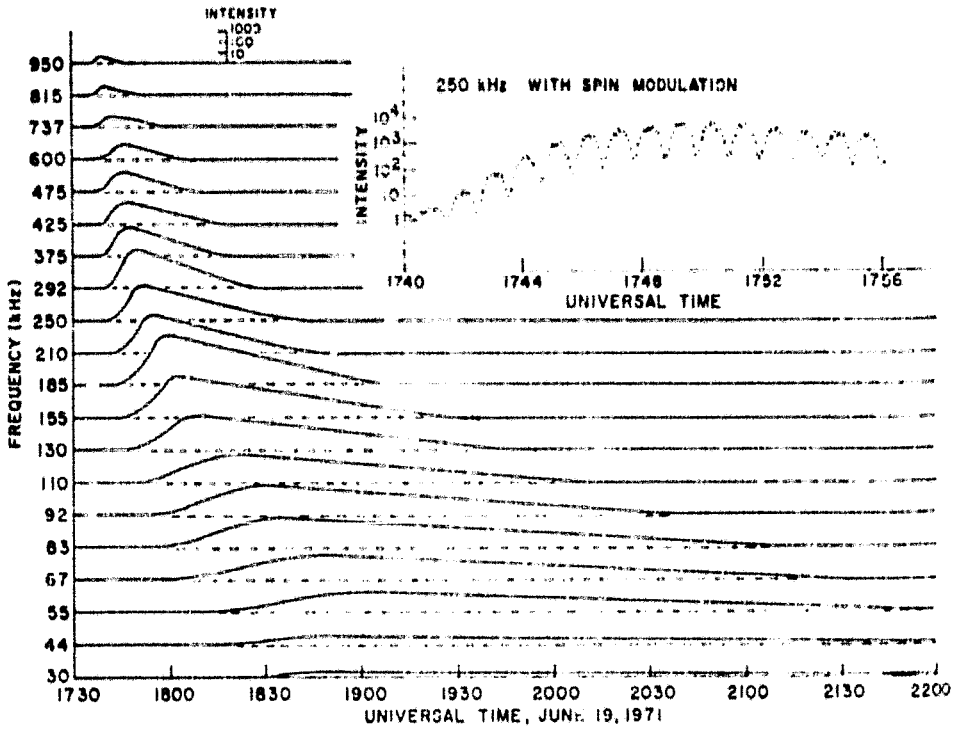

Figure 2.3

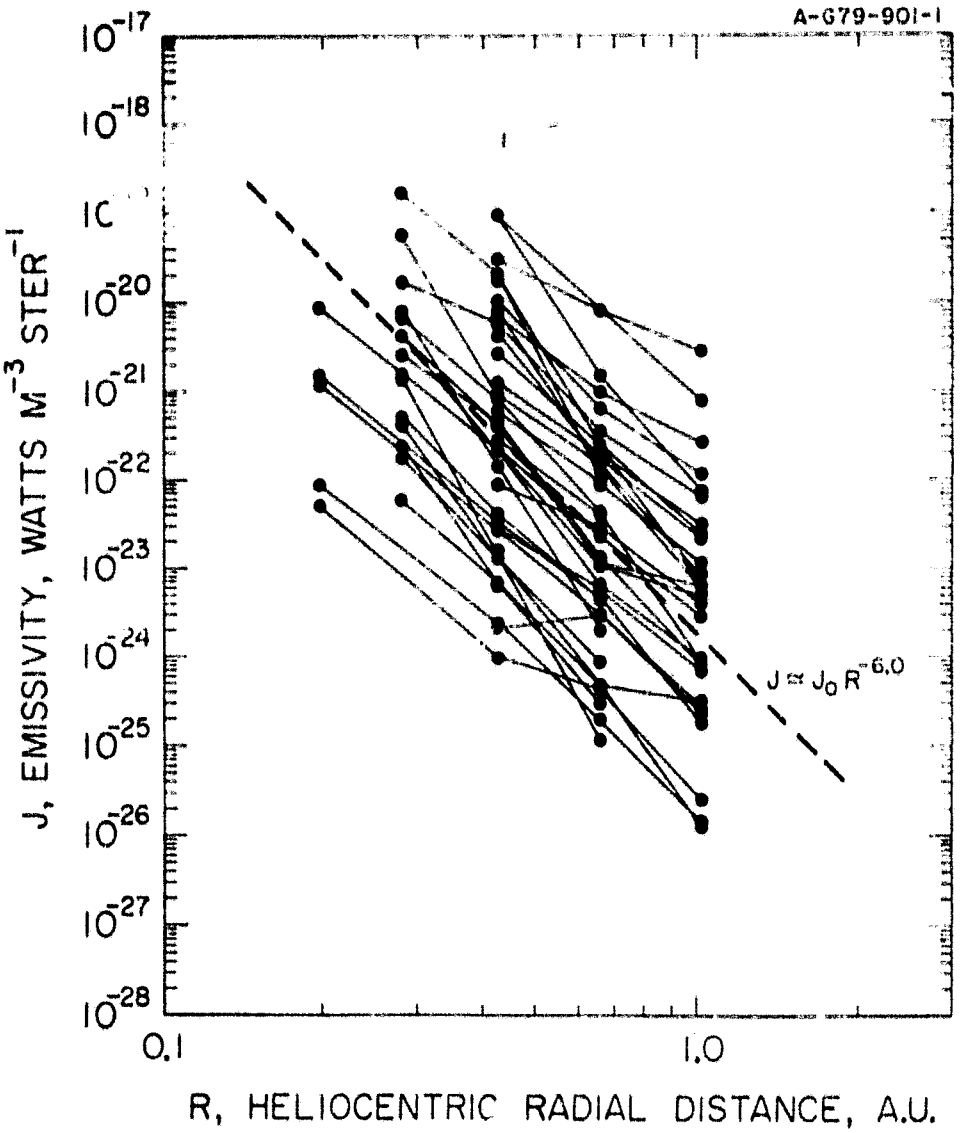
A-679-901-1
J, EMISSIVITY, WATTS M^{-3} STER^{-1}
10^{-17}
10^{-18}
10^{-20}
10^{-21}
10^{-22}
10^{-23}
10^{-24}
10^{-25}
10^{-26}
10^{-27}
10^{-28}
$J \propto J_0 R^{-6.0}$
0.1
1.0
R, HELIOCENTRIC RADIAL DISTANCE, A.U.

Figure 2.4

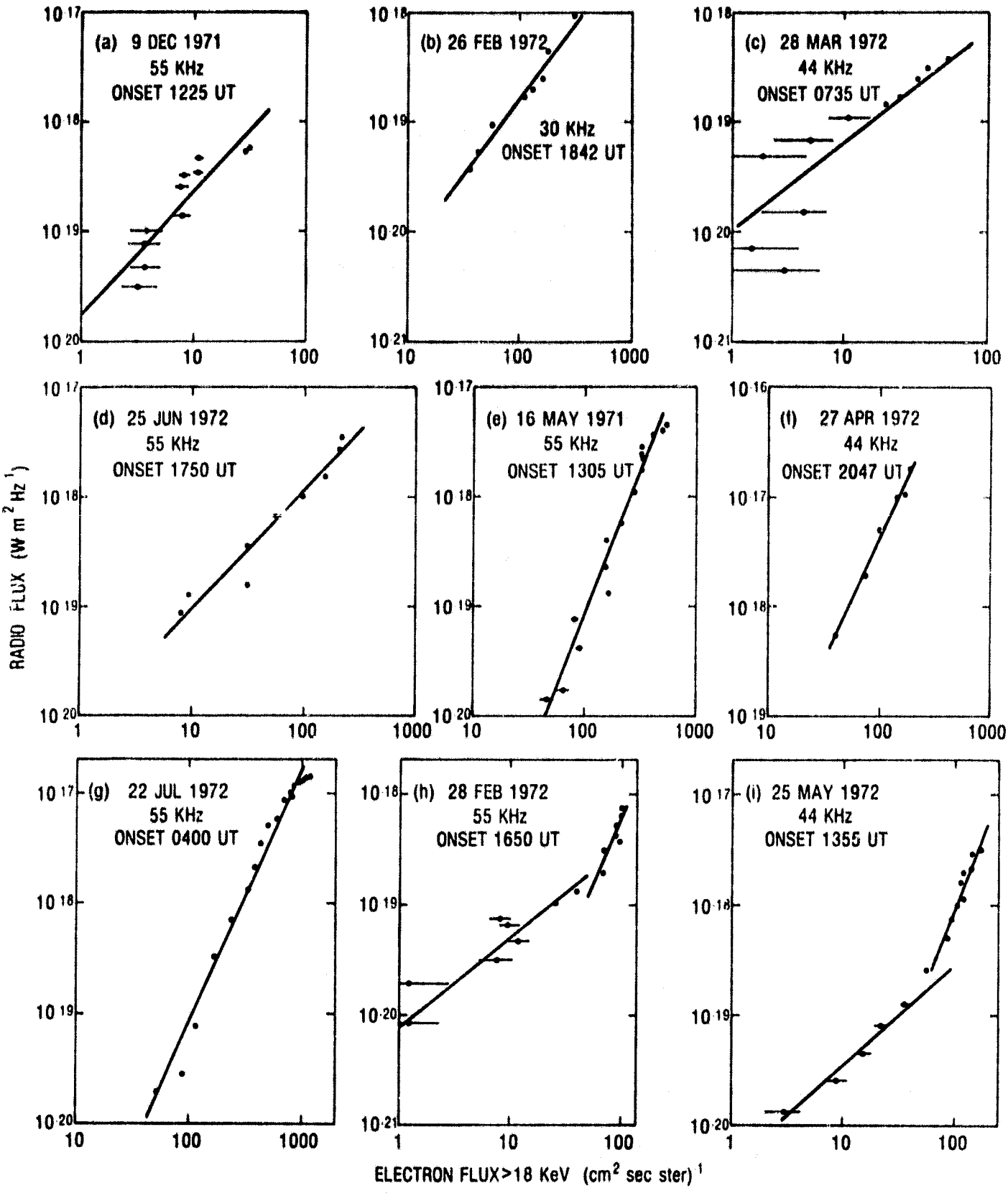
(a) 9 DEC 1971
55 KHz
ONSET 1225 UT
(b) 26 FEB 1972
30 KHz
ONSET 1842 UT
(c) 28 MAR 1972
44 KHz
ONSET 0735 UT
(d) 25 JUN 1972
55 KHz
ONSET 1750 UT
(e) 16 MAY 1971
55 KHz
ONSET 1305 UT
(f) 27 APR 1972
44 KHz
ONSET 2047 UT
(g) 22 JUL 1972
55 KHz
ONSET 0400 UT
(h) 28 FEB 1972
55 KHz
ONSET 1650 UT
(i) 25 MAY 1972
44 KHz
ONSET 1355 UT
RADIO FLUX (W m^{-2} Hz^{-1})
ELECTRON FLUX>18 KeV (cm^2 sec ster)$^{-1}$

Figure 2.5

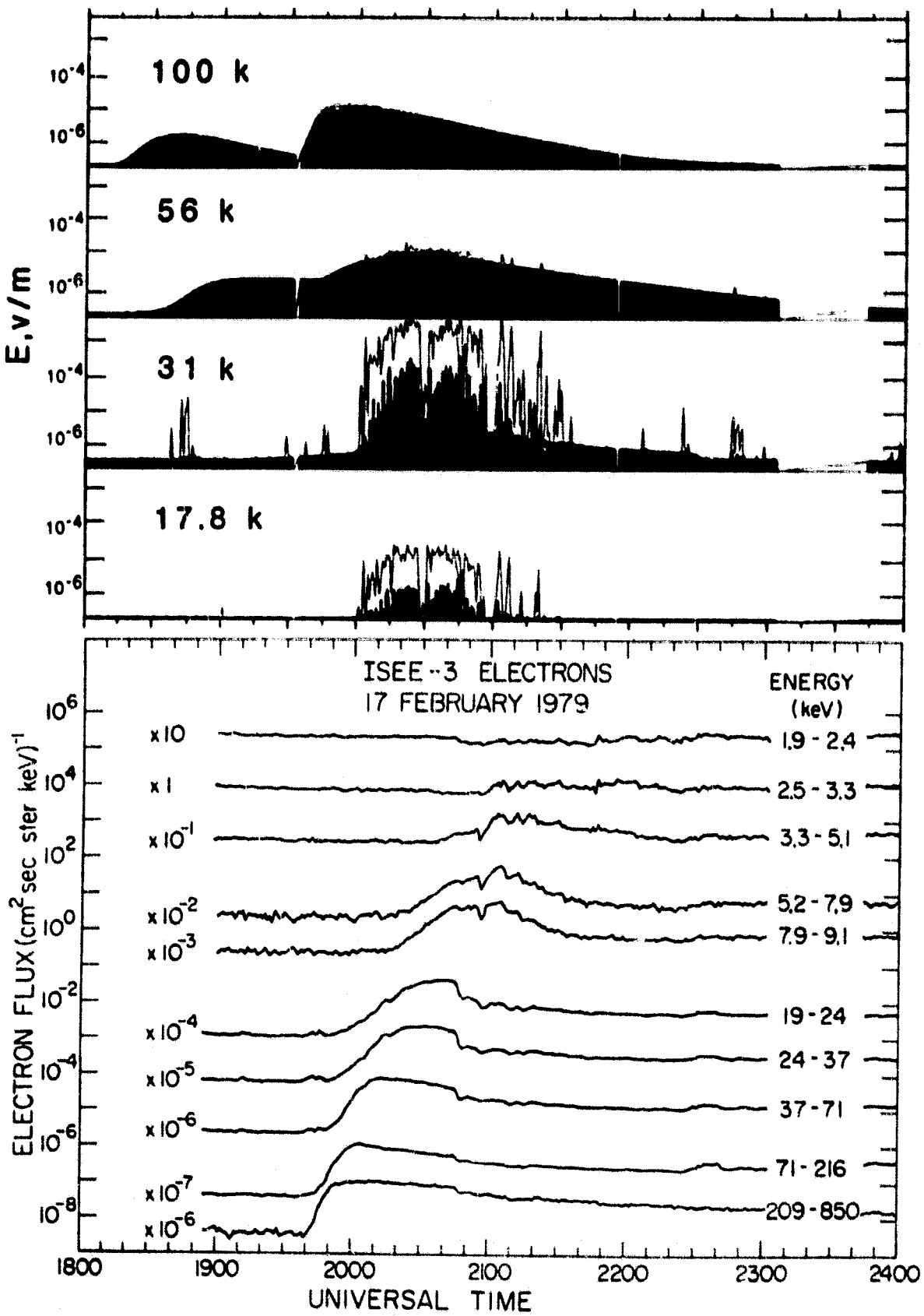
ISEE-3,FEBRUARY 17,1979
100 k
56 k
31 k
17.8 k
E,v/m
ISEE-3 ELECTRONS
17 FEBRUARY 1979
ENERGY (keV)
x10
x1
x10^-1
x10^-2
x10^-3
x10^-4
x10^-5
x10^-6
x10^-7
x10^-8
1.9 - 2.4
2.5 - 3.3
3.3 - 5.1
5.2 - 7.9
7.9 - 9.1
19 - 24
24 - 37
37 - 71
71 - 216
209 - 850
ELECTRON FLUX (cm^2 sec ster kev)^-1
1800
1900
2000
2100
2200
2300
2400
UNIVERSAL TIME

Figure 2.6

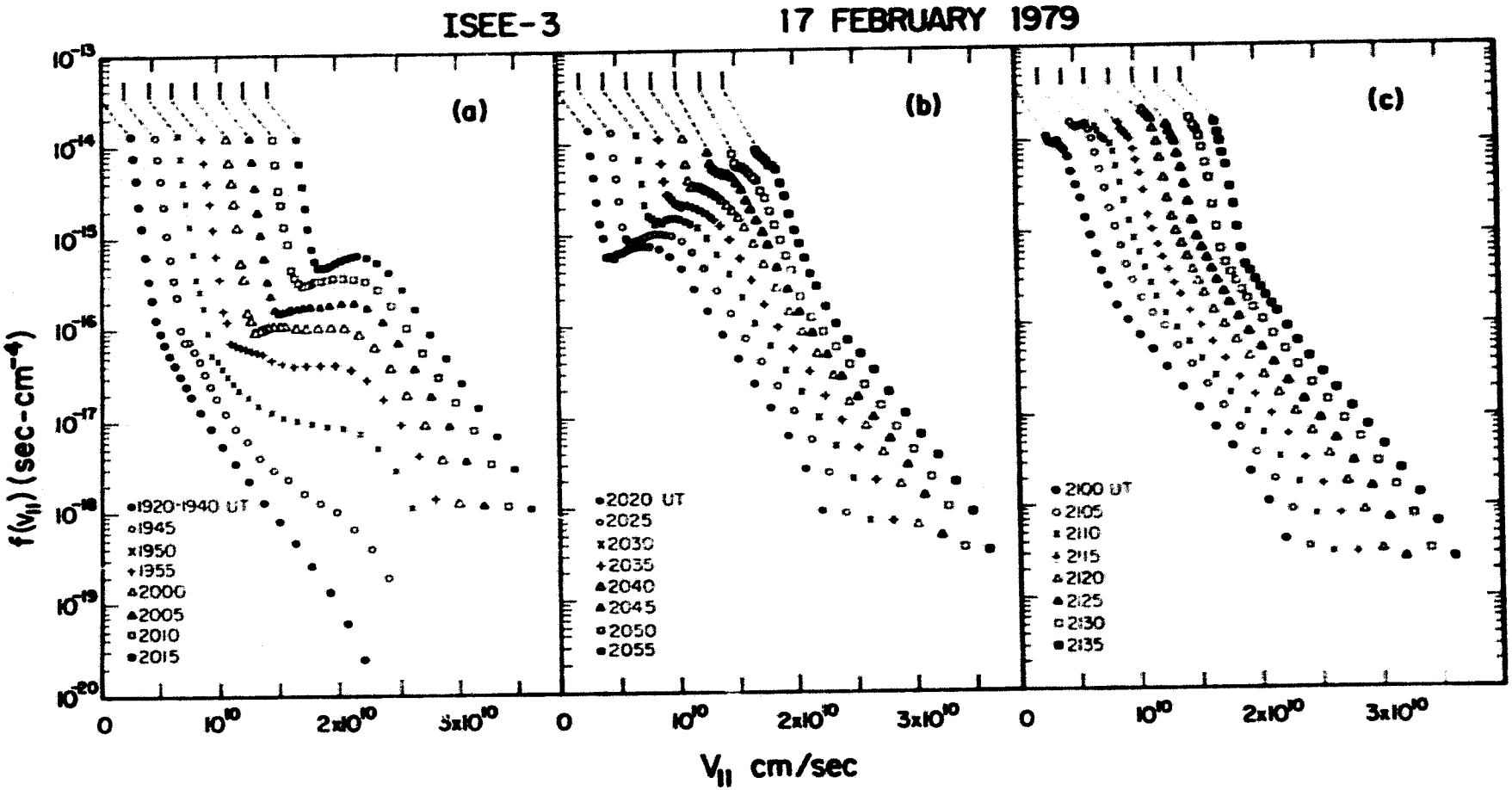
ISEE-3
17 FEBRUARY 1979
(a)
(b)
(c)
f(V||) (sec-cm⁻⁴)
V|| cm/sec
•1920-1940 UT
◦1945
x1950
+1955
△2000
▲2005
□2010
■2015
•2020 UT
◦2025
x2030
+2035
▲2040
▲2045
□2050
■2055
•2100 UT
◦2105
x2110
+2115
△2120
▲2125
□2130
■2135

Figure 2.7

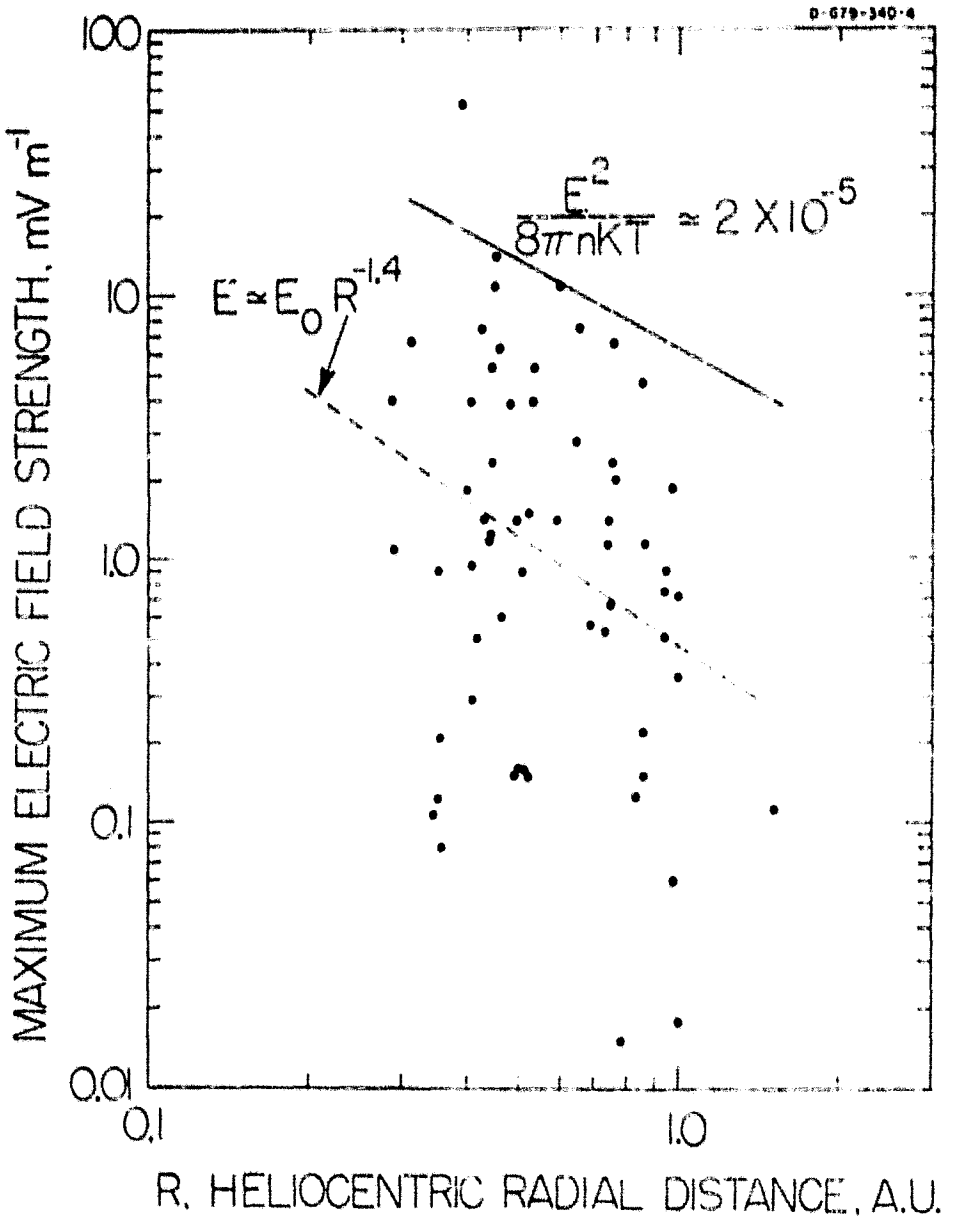
D-679-340-4
100
10
1.0
0.1
0.01
0.1
1.0
MAXIMUM ELECTRIC FIELD STRENGTH, mV m⁻¹
R, HELIOCENTRIC RADIAL DISTANCE, A.U.
E ∝ E₀ R^-1.4
E²/8πnKT ≈ 2 X 10^-5

Figure 2.8

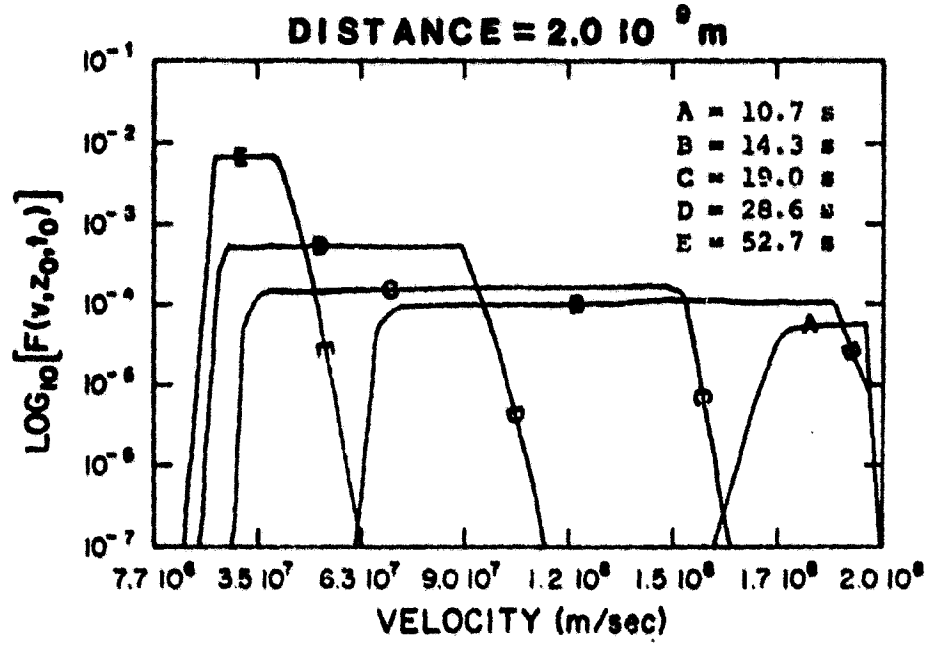
DISTANCE = 2.0 10 ⁹ m
A = 10.7 s
B = 14.3 s
C = 19.0 s
D = 28.6 s
E = 52.7 s
LOG10[F(v,z0,t0)]
10⁻¹
10⁻²
10⁻³
10⁻⁴
10⁻⁵
10⁻⁶
10⁻⁷
7.7 10⁶ 3.5 10⁷ 6.3 10⁷ 9.0 10⁷ 1.2 10⁸ 1.5 10⁸ 1.7 10⁸ 2.0 10⁸
VELOCITY (m/sec)

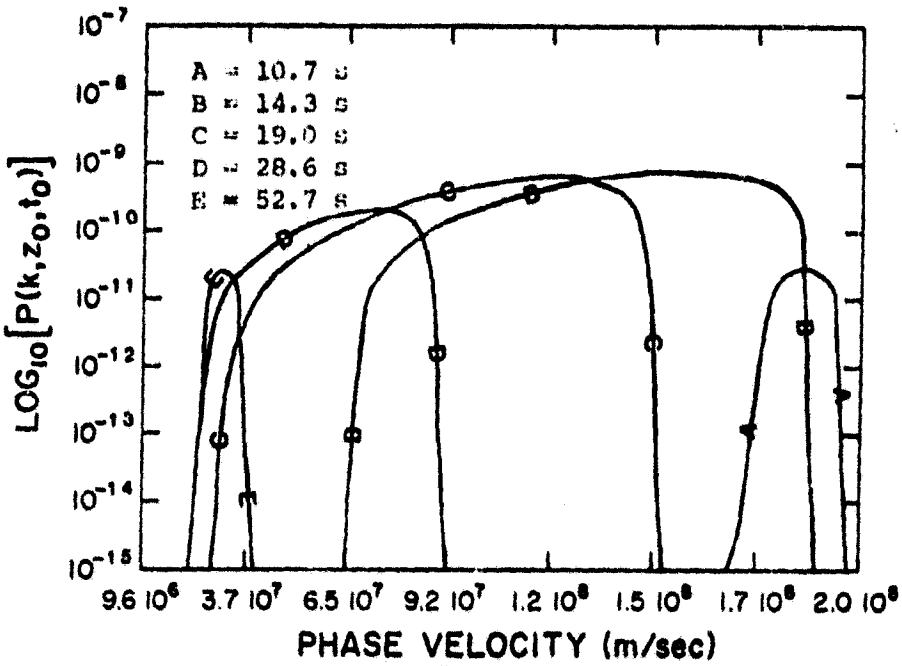
A = 10.7 s
B = 14.3 s
C = 19.0 s
D = 28.6 s
E = 52.7 s
LOG10[P(k,z0,t0)]
10⁻⁷
10⁻⁸
10⁻⁹
10⁻¹⁰
10⁻¹¹
10⁻¹²
10⁻¹³
10⁻¹⁴
10⁻¹⁵
9.6 10⁶ 3.7 10⁷ 6.5 10⁷ 9.2 10⁷ 1.2 10⁸ 1.5 10⁸ 1.7 10⁸ 2.0 10⁸
PHASE VELOCITY (m/sec)

Figure 3.1

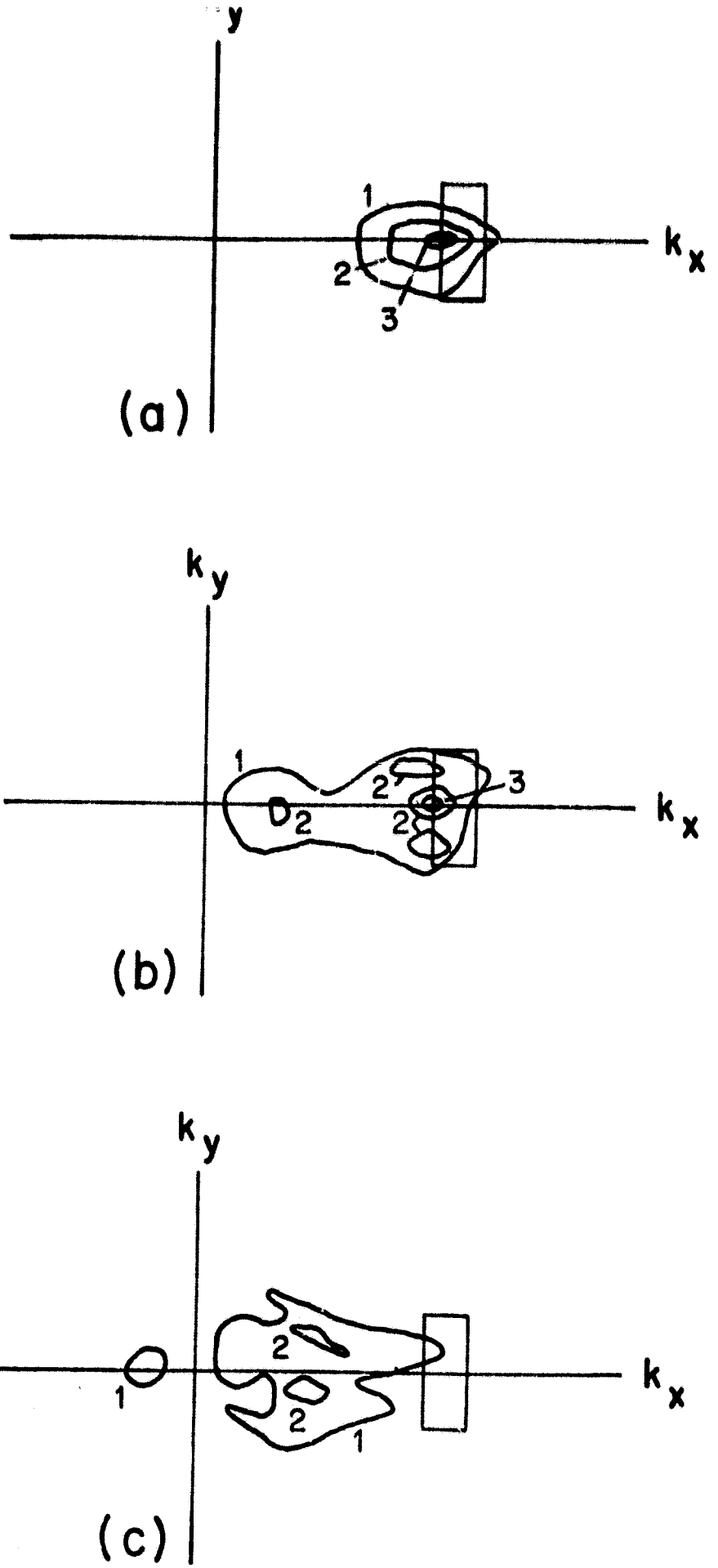

Figure 3.2

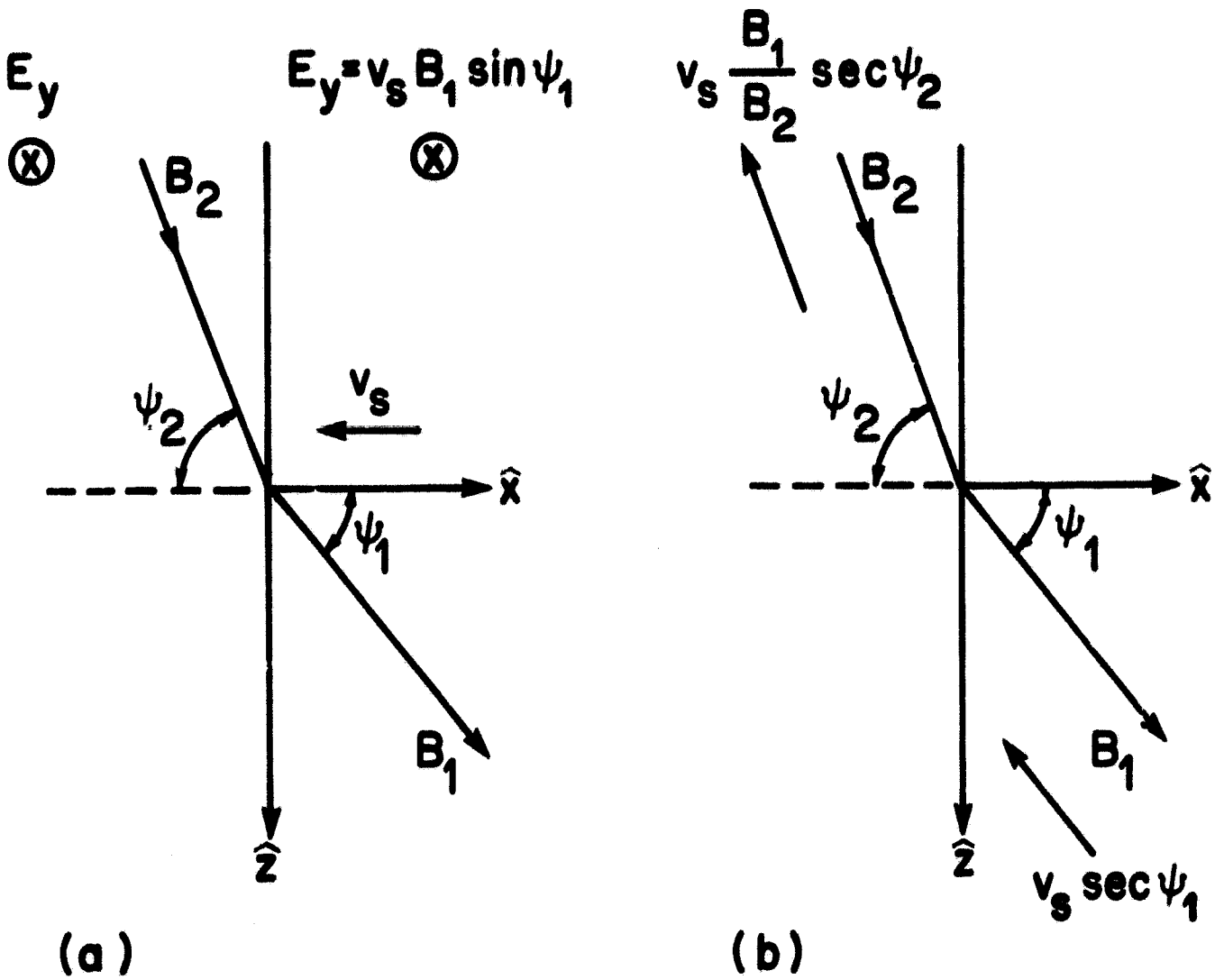
E_y
$E_y = v_s B_1 \sin\psi_1$
B_2
ψ_2
v_s
$\hat{x}$
ψ_1
B_1
$\hat{z}$
(a)
$v_s \frac{B_1}{B_2} \sec\psi_2$
B_2
ψ_2
$\hat{x}$
ψ_1
B_1
$\hat{z}$
$v_s \sec\psi_1$
(b)

Figure 4.1

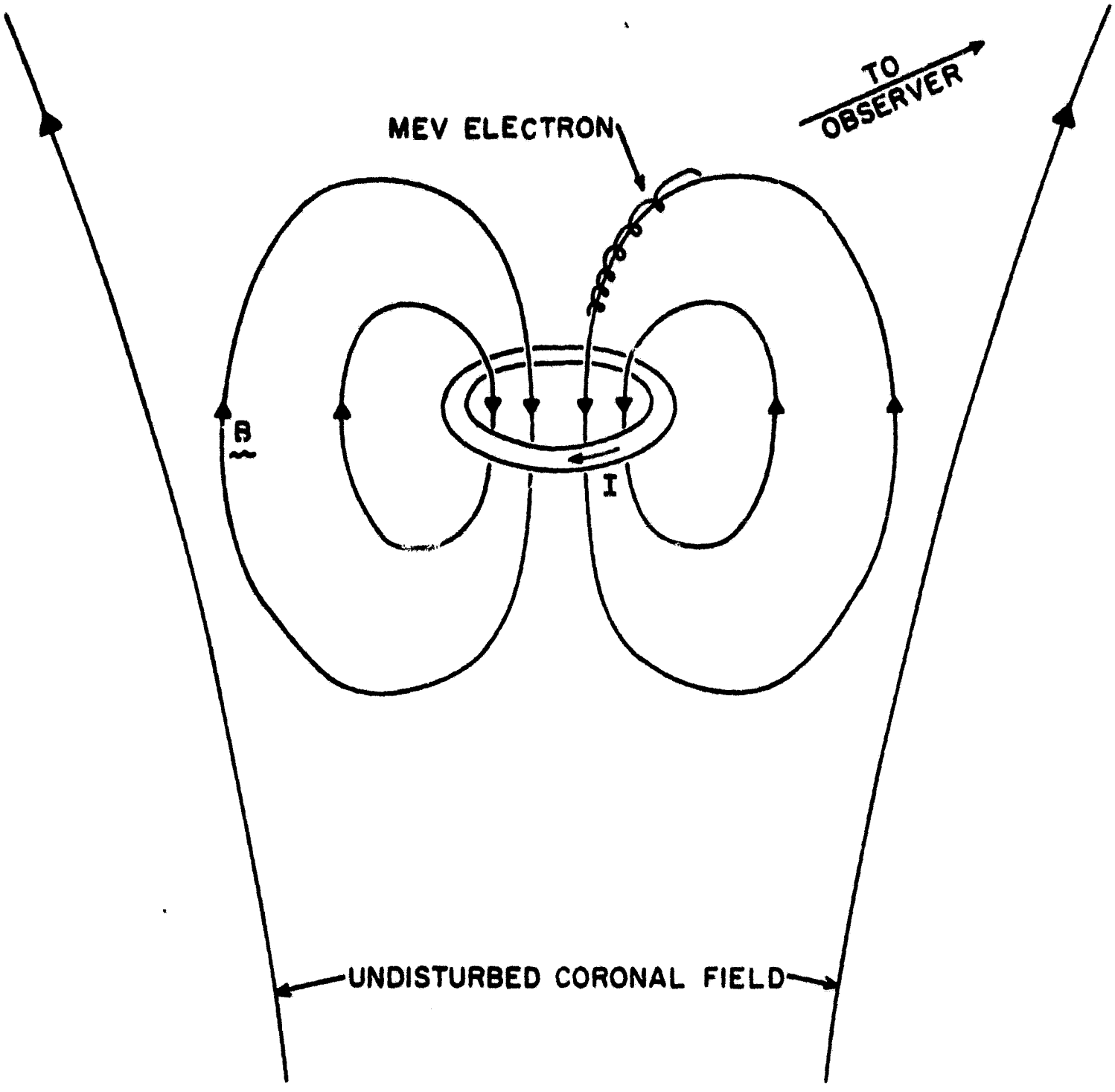

Figure 5.1

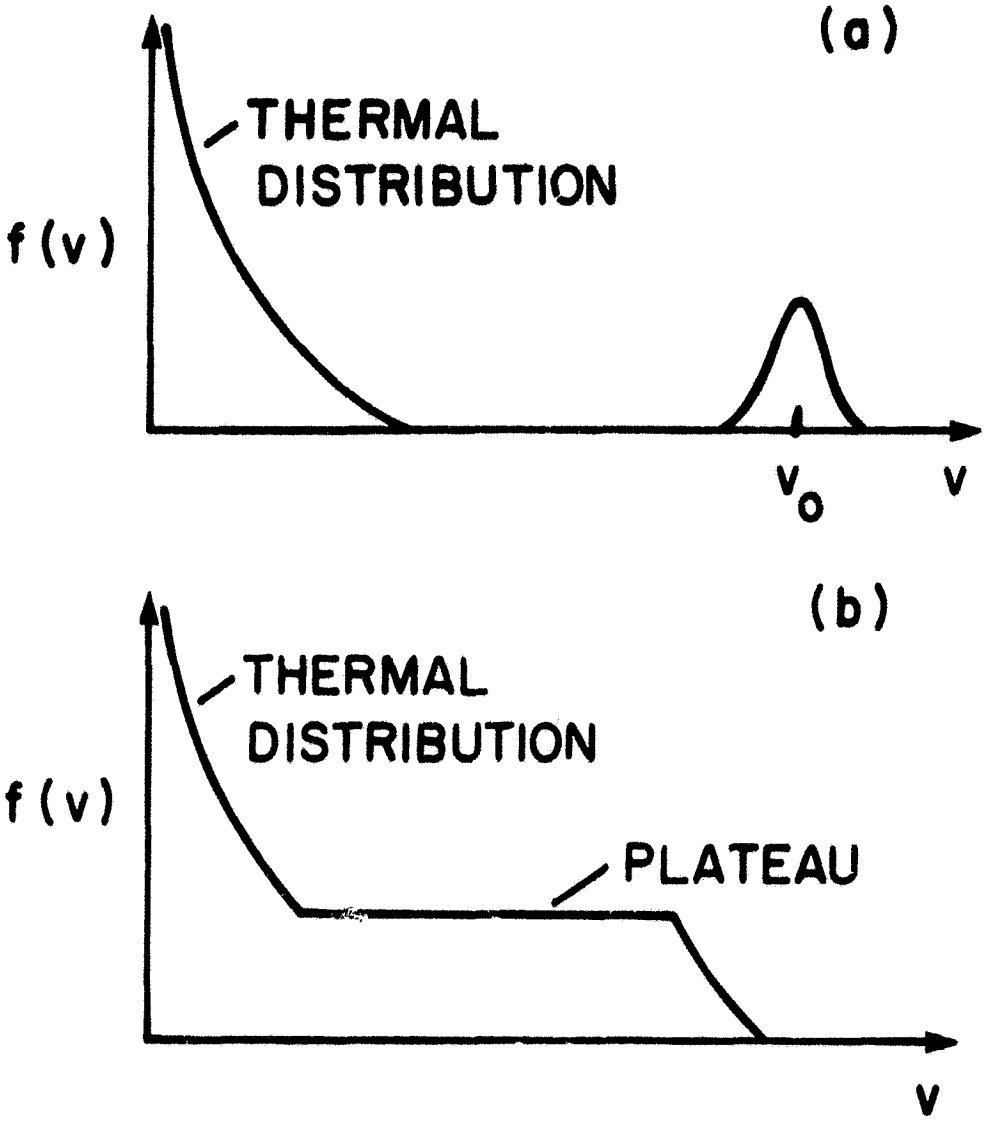
(a)
THERMAL
DISTRIBUTION
f(v)
v_o
v
(b)
THERMAL
DISTRIBUTION
f(v)
PLATEAU
v

Figure 5.2